GASEOUS INSULATION

Gases are used for high-voltage insulation and current switching in various applications such as electrical power transmission and distribution, particle accelerators, power conditioning, pulsed power systems, and overvoltage protection devices. This article is restricted to applications in electric power transmission and distribution (*T&D*) equipment in which the insulating gas is contained in grounded metallic enclosures at pressures exceeding atmospheric pressure.

Some of the advantages of gas-insulated T&D equipment, usually referred to as gas insulated switchgear, are

1. Very compact design with correspondingly low space requirements and low visual impact
2. Low equipment weight due to lightweight insulation medium
3. Protection against atmospheric disturbances on account of enclosed equipment structure
4. Controlled and controllable properties of the insulation medium
5. High personnel safety because high-voltage conductors are shielded by grounded enclosures

This article is divided in three parts, which give

1. a brief *qualitative survey* of the major features of electric power transmission and distribution systems and the associated equipment (the survey focuses on those components in which gases perform insulating and switching functions)
2. a review of the *fundamentals for the design* of gas insulation and gas switchgear,
3. a *technology outlook*, which discusses the major development trends in T&D equipment, again with focus on the role of gases

GAS INSULATION AND SWITCHING IN ELECTRIC POWER TRANSMISSION AND DISTRIBUTION

Task of Transmission and Distribution Systems

Figure 1 shows a schematic overview of the electric power T&D grid. The power generated in the power stations is fed via a generator circuit breaker and a generator step-up transformer to a high-voltage (*HV*) transmission substation, from where it is distributed by the HV transmission system. This system consists of a network of mainly air-insulated overhead transmission lines, the nodes of which are formed by HV transmission substations, which serve to control the power flow and carry out emergency operations in case of failures. Substations also channel the power via a step-down transformer into the medium-voltage (MV) distribution grid, where it is distributed by overhead lines or cables. At this level the power flow is controlled by MV substations. They direct the power directly to end users such as traction (railways) and industry or, after a further step-down transformer to the low-voltage (LV) level, to domestic applications.

The diagram gives typical ranges for the system voltages (in kilovolts), the rated currents (in amperes), and the maximal short-circuit currents (in kiloamperes) at the various voltage levels of the system. The system voltages determine the insulation design, whereas the rated and short-circuit currents determine the design of the circuit breakers.

HV and MV substations have similar basic structures: They consist of one or more busbars, which collect the arriving power and feed it to the connected lines or cables via switching units, which are referred to as switching bays in HV substations and as ring main units in MV substations (Fig. 2). A single-phase diagram of a switching unit is represented in Fig. 2(a). Its core is a circuit breaker (*cb*) connected in series with a current transformer (*ct*) and a voltage transformer (*vt*). This core unit is connected to the busbar (*bb*) and to the outgoing line or cable (arrow). The circuit breaker cb has the task of switching all currents that may occur between the busbar bb and the outgoing line/cable. The current and voltage transformers ct and vt meter the power flow through the unit and provide information for the control of the substation (see ***Switchgear protection***). The circuit breaker is connected via disconnector switches ds, which allow one to disconnect the circuit breaker unit from both busbar and line so as to configure the substation before the circuit breakers are closed. Grounding switches (*gs*) are provided to allow safe working on the unit for maintenance and repair.

Figure 2(b) shows an example of an HV switching bay for 300 kV rated voltage. The functional elements are identified by the same symbols as in Fig. 2(a). Figure 2(c) shows the structure for a MV ring main unit for 24 kV rated voltage, again with the functional elements identified. The approximate size scales of the units are indicated. The present article will be restricted to the description of the insulation and switching functions of the gas.

Gas Insulation Systems

Currently, the only gas used in gas-insulated T&D equipment is compressed SF_6. In HV transmission substations it is used at pressures of 300 to 700 kPa, and in compact MV distribution equipment at pressures of 120 to 150 kPa. The basic features of a gas insulation system are represented in Fig. 3 for the most frequently occurring case of a coaxial conductor configuration. The high-voltage conductor HV is coaxially arranged within a cylindrical grounded enclosure E and is supported by support insulators SI, which are usually made of polymer composites. The inner conductor and the support insulator are equipped with field-grading electrodes (*FGE*s), which serve to homogenize the field distribution and to reduce the field in the vicinity of the so-called triple junctions TJ where insulator, conductor, and gas meet. These locations are particularly prone to defects such as delaminations between conductor and insulator and accumulated particulate contamination, so that it is important to keep the field low enough to avoid defect-induced discharge activity.

The essential design quantity of a gas insulation system is the electrostatic field distribution within it. This field is proportional to the applied voltage and is determined by

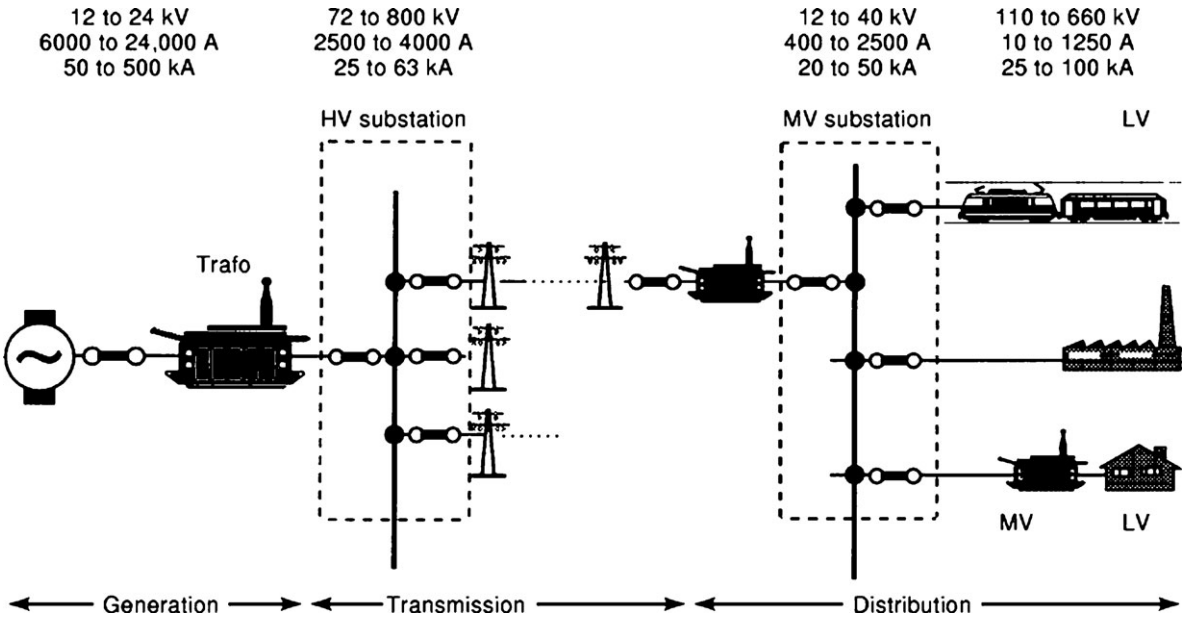

Figure 1. Structure of the electric power transmission and distribution system with generation, high-voltage (HV) transmission, medium-voltage (MV) distribution, and low-voltage (LV) distribution levels. For each level typical rated voltages, rated currents, and maximal short-circuit currents are indicated.

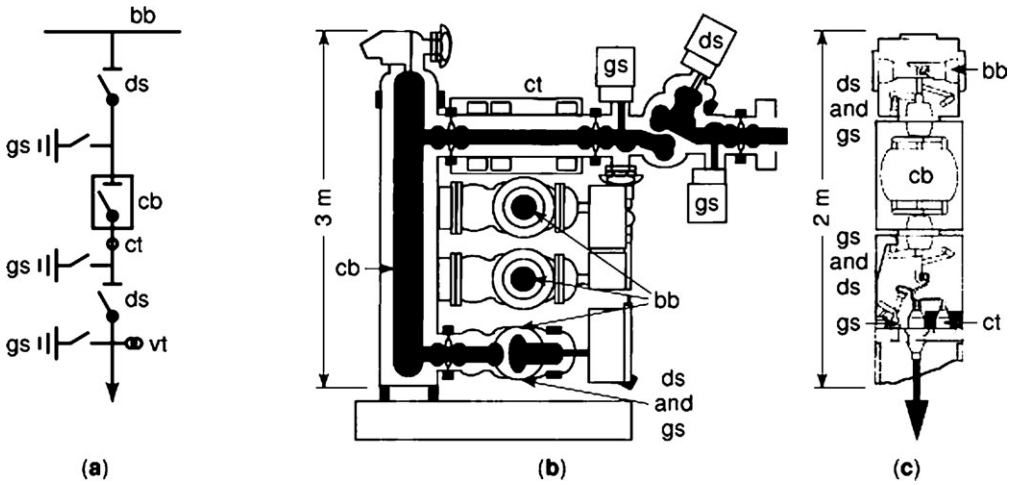

Figure 2. Structure of a functional unit of a substation: (a) single phase diagram with bb = busbar, ds = disconnector switch, gs = grounding switch, cb = circuit breaker, ct = current transformer, and vt = voltage transformer; (b) switching bay of a gas-insulated high-voltage transmission substation (GIS); (c) gas-insulated ring main unit of a medium-voltage distribution substation.

the geometry of the conductors and the support insulator and by the relative dielectric permittivity of the latter. The field can be determined numerically by standard electrostatic field calculation codes.

Performance of Gas Insulation Systems. Any insulation system must be designed for a specified rated system voltage U_0. This voltage defines a set of typical voltage stresses that may occur during system operation and that the insulation has to support without damage or failure. This performance must be verified by a set of type and routine tests. The most important test voltages are the operating voltage, transient voltage surges caused by switchgear operation (*SI* = switching impulse due to circuit breaker operation, *VFT* = very fast transients due to disconnector operation) and lightning surges caused by atmospheric disturbances (*LI* = lightning impulse). Details on these test voltages can be found in the article on insulation testing.

Design of Gas Insulation Systems. An insulation system is designed for a prescribed voltage beyond which the electric field in the system might initiate damage or failure. The corresponding field values are referred to as *design fields*. For a chosen solid insulation material, gas, and gas pressure, the design of a gas insulation system thus consists in optimizing the electrode geometry so that the design fields

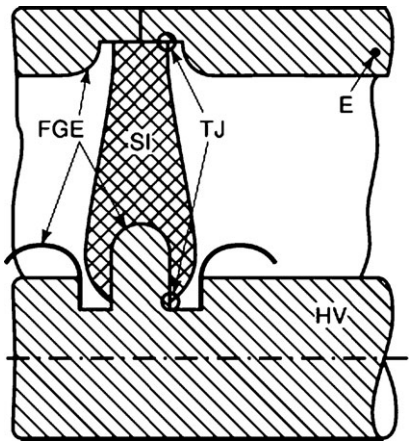

Figure 3. Structure of coaxial gas insulation system: HV = high voltage conductor, E = grounded enclosure, SI = support insulator, FGE = field grading electrodes, TJ = triple junction between electrode, solid insulator, and gas.

are not exceeded at any location when the test voltages are applied.

If the insulation system were ideally smooth and free of contaminants, the design fields in the gas could be chosen equal to the critical field E_c of the gas, i.e. the field at which ionization sets in. For most gases, E_c is proportional to the molecular particle density n or, for a given temperature T, to the gas pressure p. Molecular density n and pressure p are related by the gas kinetic equation $p = nkT$, where $k = 1.4 \times 10^{-23}$ J/K is the Boltzmann constant. The critical field can thus be expressed as

$$E_c = (E/n)_c n = (E/p)_c p \quad (1)$$

where $(E/n)_c = (E/p)_c/(kT)$ is a gas-specific property. Values of $(E/n)_c$ and $(E/p)_c$ at ambient temperature are given in Table 1 for air and SF_6. For solid insulating materials similar critical field values exist.

Real insulation systems are not ideal. They may contain various kinds of small-scale defects that locally enhance the electric field. Such defects are never entirely avoidable during manufacture and assembly, but their size can be kept below certain limits by adequate quality control. Typical examples of defects in gas-insulated systems are

- The roughness of electrode surfaces, which consists of microscopic surface protrusions, at which the field is locally enhanced
- Small conducting particles, which are oriented along the electric field and moved around by electrostatic forces
- Small voids in the solid insulators and close to the electrodes to which they are molded

The unavoidable presence of such defects must be accounted for in the insulation design and requires that the design fields be chosen below the ideal limit of the critical field E_c of the gas by a factor which has to be selected according to uncontrollable defects. Such reduced design fields E_0 are referred to as defect-tolerant design fields and are best expressed in terms of the critical field E_c as the ideal limit:

$$E_0/E_c = f(\text{defect type, defect scale, gas pressure, ...}) < 1 \quad (2)$$

The dimensionless reduction factor f generally depends on the defect type, its length scale, the gas pressure, the applied voltage waveform, and various other parameters. This dependence will be referred to as the design field relation and has to be derived from discharge models or through experiment.

An overview over basic gas discharge phenomena can be found in Ref. 1. For the technical aspects of gas insulation the reader is referred to Refs. 2 and 3.

Gas Switchgear

As shown in Fig. 2(a), a substation unit requires several types of switchgear with different tasks. Of these, the circuit breaker is subject to the highest performance requirements because it must interrupt the full range of currents that may occur in the system, ranging from small capacitive and inductive currents, through rated currents and out-of-phase currents, up to short-circuit currents. For this reason, circuit breakers require the highest design effort and will form the main subject of this article. Disconnector and grounding switches only have to handle very small currents, so that arcing in them has a negligible effect. They can normally be designed by standard mechanical and gas insulation design principles and will not be discussed in detail.

Performance of Circuit Breakers. The main performance characteristics of a circuit breaker are:

1. The rated voltage, which determines the open-contact insulation, capacitive current, and short-circuit current interruption requirements.
2. The maximal short-circuit current to be interrupted, which determines the arcing design.
3. The rated current carrying capability, which determines the thermal contact design.

Figure 4 gives an overview of the voltage and short-circuit current performance of some common circuit breaker types used in T&D systems. Magnetic circuit breakers (*MCB*) operate in ambient air up to voltages of typically 12 kV and currents of 100 kA. Vacuum circuit breakers (VCB, see vol. 21, p. 196) operate at the MV distribution level, typically up to about 36 kV and 40 kA and have a development potential to higher currents and voltages. SF_6 circuit breakers using a combination of piston compression and self-blast pressure generation serve the full range from distribution to transmission and generator switchgear. At the distribution level they operate at 12 to 36 kV with short circuit currents up 40 kA, typically. At the high voltage transmission level they operate up to 800 kV and 63 kA, the voltage performance above about 300 kV being obtained by series connection of interrupter units. SF_6 generator breakers operate at 12 to 24 kV up to 160 kA with a development trend to higher currents.

Table 1. Integral Parameters for the Approximate Description of Gas Discharge Processes in Gas Insulation

				Numerical values[1]	
Parameter	Symbol	Unit	Approx. scaling	SF_5	Air
Particle-density-reduced critical field	$(E/n)_c$	$V{\cdot}m^2$	Const.	3.6×10^{-19}	1×10^{-19}
Pressure-reduced critical field at 20°C	$(E/p)_{c0}$	$V \cdot m^{-1} \cdot Pa^{-1}$	Const.	89	25
Pressure reduced effective ionization coefficient	α/p	$(m\,Pa)^{-1}$	$\alpha/p \approx c\,[(E/p) - (E/p)_{cr0}]^{\beta}$	$\beta \approx 1c \approx 2.8 \times 10^{-2}$	$\beta \approx 2c \approx 0.74$
Logarithim of critical avalanche charge	K_z	–	Const.	10.5(+)	9(+)
Reduced background field required for streamer propagation	$\gamma = E_p/E_c$	–	Const.	1(+)1(−)	−0.17(+)−0.5(−)
Leader inception corona charge	Q_1	A·8	$Q_1 \propto c\,p^{-n}$	$n = 2c \propto 50(+), 500(-)$	
Toepler constent	k_T	$V \cdot s \cdot m^{-1}$	Const.	$(4\text{ to }8) \times 10^{-3}$	$(5\text{ to }6) \times 10^{-3}$

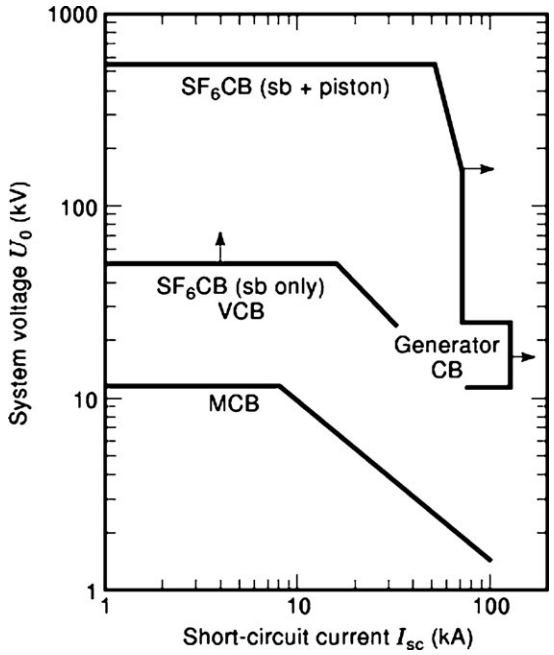

Figure 4. Voltage and short-circuit current interruption performance of various types of circuit breakers used in T&D: VCB = vacuum circuit breakers, SF_6 CB = SF_6 circuit breakers, MCB = magnetic circuit breakers, sb = self-blast.

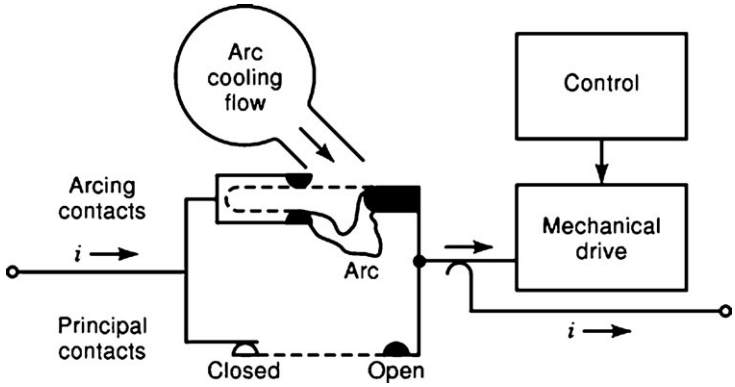

Figure 5. Functional scheme of a gas circuit breaker with principal and arcing contacts in parallel: i = current.

Design of Gas Circuit Breakers. The design of gas circuit breakers comprises four major aspects:

1. Mechanical design of the enclosure and the contact motion system
2. Design of the insulating system
3. Thermal design for the ohmic heat dissipated by the rated current
4. Arc design

In the present article focus will be on arc design, which is the main factor determining the breaker's structure. The discussion will be restricted to SF_6 as arc-interrupting medium. Qualitatively, most of the statements made for SF_6 are also valid for other gases. Other interrupting media, such as compressed air, are only of historical interest and are treated in detail in Ref. 4 and 5.

A functional scheme of a gas circuit breaker is shown in Fig. 5. The breaker consists of a mechanical drive that is actuated by a control system, a contact system, and a flow-generating system to provide arc cooling. The contact system normally consists of two separate contact pairs: the principal contacts and the arcing contacts. The principal contacts carry the current when the breaker is closed, and the arcing contacts carry the current during the interruption process. The two contact pairs are mechanically synchronized as schematically shown in the figure. During opening of the breaker the current is first commuted from the principal contacts to the arcing contacts, which are separated with delay after the current has been completely transferred. When the breaker is closed, the arc contacts close first to handle pre-arcing. In this way, erosion of the principal contacts due to arcing is minimized to keep the contact resistance low for carrying the rated current. The arc cooling flow system is only represented schematically and provides a gas flow to cool the arc during the interruption process.

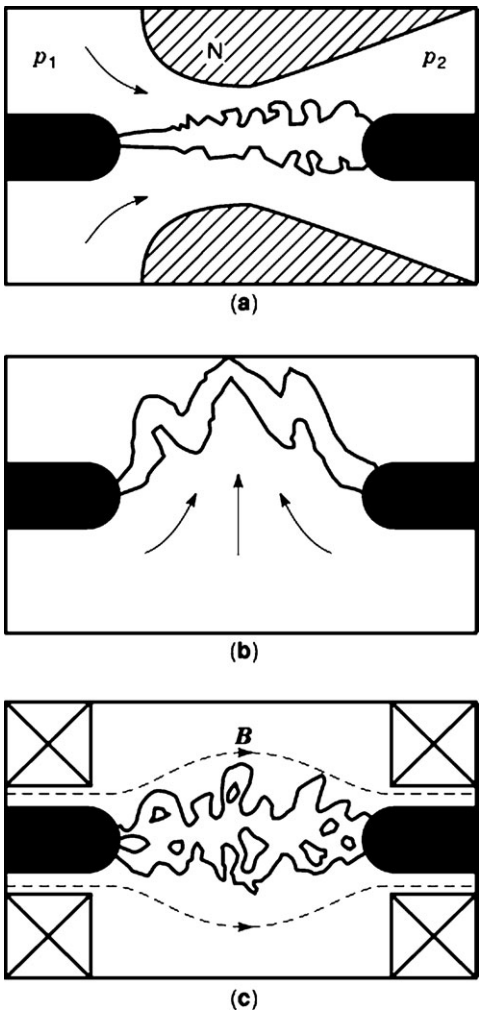

Figure 6. Basic arc cooling mechanisms: (a) cooling by axial flow generated in a nozzle N by a pressure difference $p_1 - p_2$ (b) Transverse, or cross-flow, cooling; (c) Cooling by turbulence due to magnetohydrodynamic destabilization of the arc by an axial magnetic field $\boldsymbol{B}$.

The three main arc cooling mechanisms used in SF_6 breakers are schematically represented in Fig. 6.

The most frequently used mechanism is a gas flow parallel to the arc, which is usually referred to as *axial flow* [Fig. 6(a)]. It is generated by applying a pressure difference $p_1 - p_2$ across a nozzle N along the axis of which the arcing contacts are separated. Arc cooling in this configuration is achieved by a combination of axial convection and radial turbulent heat transfer by the turbulence excited at the arc–gas boundary.

The second cooling mechanism is a flow perpendicular to the current flow in the arc, which is usually referred to as *cross flow* [Fig. 6(b)]. Here, the arc is cooled by a combination of transverse convection and turbulent heat transfer, the turbulence being mainly generated by magnetohydrodynamic arc instabilities. The cross-flow is usually generated by moving the arc perpendicular to the current flow through the gas with the help of a magnetic field, which exerts Lorentz forces on the arc current.

The third cooling mechanism is the excitation of turbulence by *magnetohydrodynamic instabilities*, which are generated by a magnetic field $\boldsymbol{B}$ parallel to the arc current flow [Fig. 6(c)].

Some circuit breaker concepts use only one of the above cooling mechanisms; others use combinations of them.

Figure 7 shows some of the most frequently applied SF_6 circuit breaker types in some more detail.

In the so-called *puffer* or *piston breaker* [Fig. 7(a)] the principal contacts FPC and MPC are arranged concentrically around the arcing contacts FAC and MAC, which normally have a rod-and-tulip shape. When the breaker opens, the mobile contact system MAC and MPC is driven, together with the insulating nozzle N, against a fixed annular piston FP so that the gas in the volume CV is compressed. The overpressure thus generated causes a gas flow through the nozzle along the axis of the arc, which is drawn between the arcing contacts FAC and MAC. The puffer breaker is thus of the axial flow type according to Fig. 6(a).

Figure 7(b) shows a simplified scheme of a so-called *self-blast breaker* in which the principal contacts have been omitted for simplicity. In this design the overpressure for driving the gas flow is generated by the arc itself. Part of the arc plasma and arc-eroded vapor from the nozzle N are injected into the high-pressure volume HPV during the high-current phase. This injection is associated with an input of thermal energy into the volume HPV, which results in a pressure rise. When the current goes to zero, the heating effect of the arc ceases and the overpressure accumulated in the volume HV starts a reverse flow through the nozzle N into the exhaust volume EV, which cools the arc axially according to Fig. 6(a).

Figure 7(c) shows a modification of the concept of Fig. 7(b) that is usually referred to as the *magnetically enhanced self-blast breaker*. In this concept the plasma injection into the high-pressure volume HPV is enhanced by magnetic rotation of the arc section upstream of the nozzle N. A magnetic field $\boldsymbol{B}$ with a radial component is generated in the arc zone by a coil C, which is connected into the current path. This field acts on the arc current and exerts an azimuthally directed Lorentz force, which drives the arc rotation. The centrifugal forces created by the rotation enhance the radial plasma injection into the volume HPV. When current zero is approached, the centrifugal forces cease and the flow is reversed, providing arc cooling by axial flow according to Fig. 6(a).

Figure 7(d) shows a breaker type usually referred to as the *arc spinner*. In this concept, again a magnetic field $\boldsymbol{B}$ is generated by a coil C, the radial component of which rotates the arc azimuthally. The cooling gas flow consists in the relative motion of the arc with respect to the surrounding gas, which is experienced as transverse gas flow by the arc in its own system of reference and which corresponds to a cross flow cooling mechanism according to Fig. 6(b). Additionally, the axial component of the magnetic field $\boldsymbol{B}$ excites magnetohydrodynamic instabilities, thus providing an additional turbulent cooling mechanism according to Fig. 6(c).

A general overview of circuit breaker technology can be found in textbooks (4, 5). SF_6 circuit breakers are specifically treated in Ref. 6.

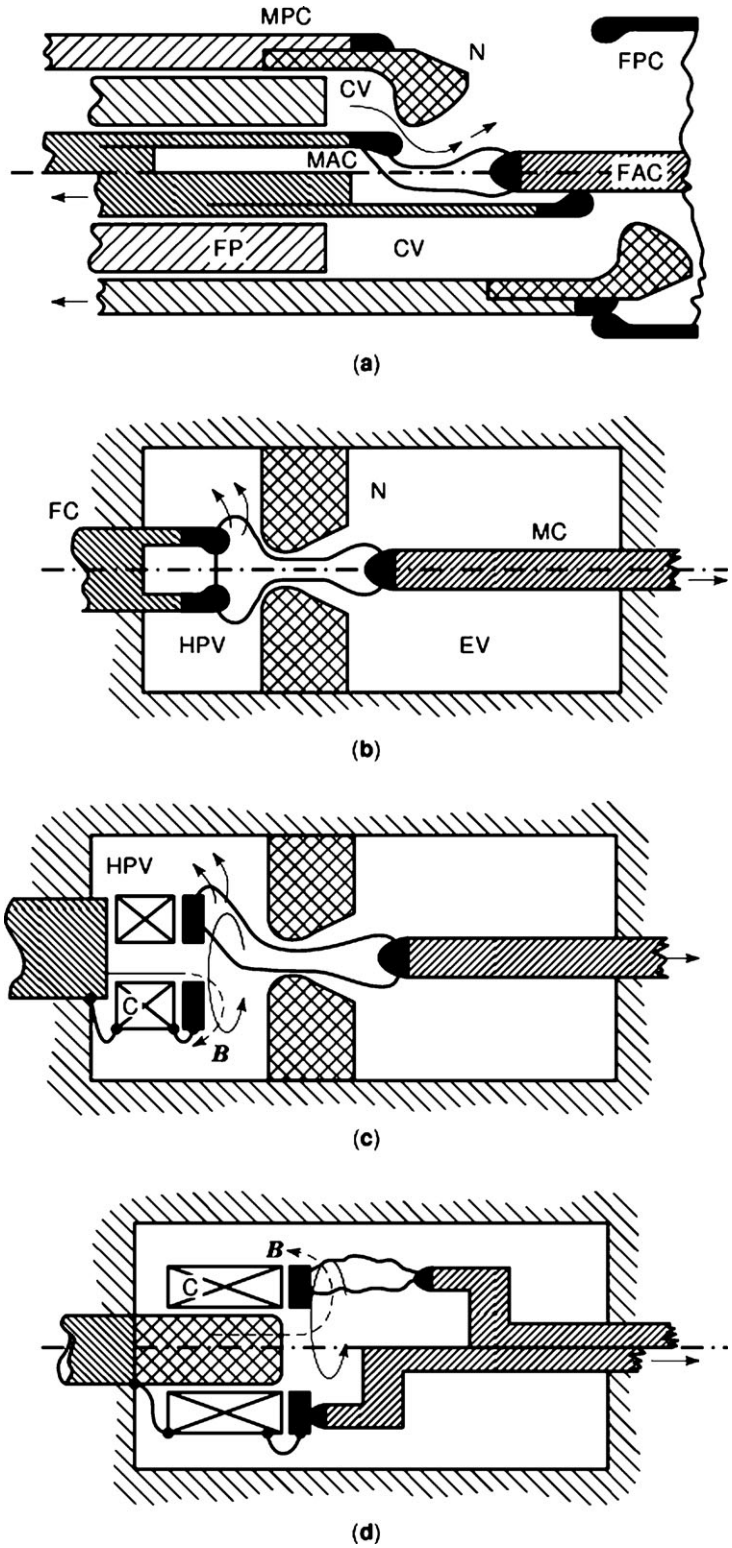

Figure 7. Major types of SF_6 circuit breakers: (a) piston or puffer breaker with MPC = mobile principal contact, FPC = fixed principal contact, N = nozzle, CV = compression volume, FP = fixed piston, MAC = mobile arcing contact, FAC = fixed arcing contact; (b) self-blast circuit breaker (only arcing contact system shown) with FC = fixed contact, MC = mobile contact, HPV = high-pressure volume, N = nozzle, EV = exhaust volume; (c) magnetically enhanced self-blast breaker (only arcing contact system shown): coil C generates magnetic field $\boldsymbol{B}$, which causes arc rotation to produce centrifugal arc plasma flow, which enhances pressure buildup in high-pressure volume HPV; (d) arc spinner: coil C generates magnetic field $\boldsymbol{B}$, which rotates arc azimuthally through the gas so that it experiences a transverse flow; additional arc destabilization by axial magnetic field component.

GENERAL DESIGN PRINCIPLES FOR GAS INSULATION

Gas discharge physics has been a very intensive field of research in the last three decades and has attained a level of understanding that allows us, to a large extent, to base the design of gas insulation systems on physical principles instead of traditional trial-and-error engineering. Therefore we will describe, instead of design details, the physical principles underlying gas insulation design. These principles can be discussed in general terms without reference to specific gases and gas pressures and allow us to derive general gas insulation design principles. SF_6 specific issues will be treated in a special section. Other insulation gases will be discussed briefly in the technology outlook section.

Gas Discharge Physical Concepts

Under the specific conditions of gas-insulated systems (weakly nonuniform electric fields, gas pressures above atmospheric, voltage stress ranging from continuous ac or dc to switching-induced overvoltage transients) their performance limits are controlled by a number of discharge mechanisms, which are schematically represented in Fig. 8 in order of increasing intensity from left to right. The gas properties required for the quantification of these processes are described in detail in ***Conduction and breakdown in gases***. For an approximate treatment, they can be summarized in the form of integral parameters, a selection of which is listed in Table 1, where also numerical values are given for SF_6 and air, as examples. The significance of these parameters will be discussed below. It should be noted that aging of gas-insulated systems does not occur if discharges are avoided.

First Electron Generation. Most gas discharge processes require for their initiation an electron that starts the first ionization avalanche. This effect is usually quantified by the rate at which first electrons are produced in a specific discharge configuration. The reciprocal of this rate gives the average statistical time lag between the instant at which the discharge criterion is fulfilled and the actual start of the discharge.

For positive polarity discharges, field detachment from negative ions in the gas is the dominant electron generation mechanism [Fig. 8(a)]. The rate of this process is controlled by the volume density of detachable negative ions in the gas and strongly increases with the electric field, so that the volume of the region within which the field is high is a key quantity. For negative polarity discharges, field emission from the cathode is usually dominant, so that the field and the emissive properties at the cathode are the controlling parameters.

Statistical time lags play a decisive role for short-duration voltage stresses such as LI and VFT overvoltages, where they determine the average level and the statistical scatter of the breakdown voltages; see ***Conduction and breakdown in gases***.

Subcritical Discharges. This notion is understood to comprise all discharge mechanisms occurring below the voltage level at which self-propagating discharge processes like

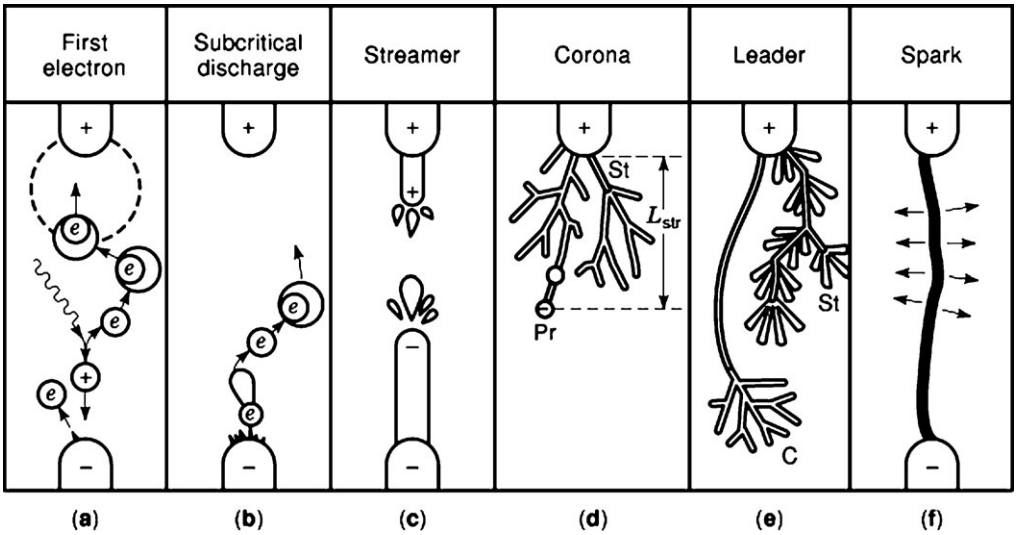

Figure 8. Schematic representation of major gas discharge mechanisms arranged in order of increasing intensity from left to right. (a) First electron generation by emission from cathode, photoionization in the gas volume, and field detachment from negative ions in the vicinity of the anode. (b) Subcritical discharge activity: drift of ions generated by cathodic electron emission, subcritical avalanching, and subsequent attachment to electronegative molecules. (c) Streamer discharge with schematic indication of avalanches feeding the propagating streamer tip. Streamer channel diameter is smaller for positive polarity due to converging avalanches. (d) Corona as branched streamer system of length scale L_s. Stem (St) and precursor (Pr) as main mechanisms for leader inception. (e) Leader discharge: Continuous propagation mode controlled by stem mechanism with tip corona C. Stepped propagation mode St controlled by precursor mechanism. (f) Spark breakdown with expanding plasma channel.

streamers can be generated. One example is the emission of electrons from microscopic cathode asperities, possibly amplified by local avalanching, which are subsequently attached to neutral atoms and drift as ions through the insulation gap under the effect of the electrostatic field [Fig. 8(b)]. A similar drift process may occur with microparticles (dust) that have been charged by contact with an electrode. For the quantification of subcritical discharges the charge carrier production rates and their mobilities are required. For a more detailed discussion see ***Conduction and breakdown in gases***.

In spite of their low current levels, subcritical discharges may have significance for gas insulation when the charge carriers drift to insulator surfaces and accumulate there. Such a surface charge accumulation may distort the electric field and trigger stronger discharges. This effect can be particularly important in dc insulation.

Streamers. The streamer mechanism is a self-channeling and self-propagating ionization processes [Fig. 8(c)], which is discussed in detail in the article on ***Conduction and breakdown in gases***. Some characteristics of streamers are polarity-dependent, mainly due to the polarity dependence of the channel diameter: Positive (cathode-directed) streamers are smaller in diameter than negative streamers, due to the focusing action of the converging avalanches by which the streamer head propagates.

The main integral parameters required for the quantification of the streamer process are the critical avalanche size above which streamers are initiated, the minimal background field E_p required for streamer propagation, and the streamer propagation velocity V_s. The critical avalanche size is expressed as the natural logarithm K_s of the critical number of electrons in the avalanche. Numerical values for K_s and E_p are given in Table 1. For details of the streamer process, see ***Conduction and breakdown in gases***.

Streamer inception is controlled by a critical avalanche criterion of the general form.

$$\int \alpha[E(x), n]dx > K_s \tag{3}$$

where $\alpha(E, n)$ is the field and particle density dependent effective ionization coefficient and $E(x)$ the electric field distribution along the streamer path. For the practical application in gas insulation systems, a special form of the streamer criterion can be derived by expressing the field distribution $E(x)$ in the vicinity of an insulation defect in terms of the undisturbed background field E_0 at the defect location and the scale of the defect (7). The streamer inception criterion can then be written in the general form

$$E_{0s} = E_c f_s(\text{gas, defect type}, pl, \epsilon_r, \text{ form of defect}, \ldots) \tag{4}$$

Where E_{os} is the background field at which streamer inception criterion is fulfilled when a defect of scale l is present. The reference field E_c is the critical field of the gas. The dimensionless factor f_s depends on the gas, the defect type, the product pl of gas pressure p and major defect scale l, the relative permittivity ϵ_r of the insulating material in the vicinity of the defect, and further dimensionless parame-

ters that characterize the form of the defect. The factor f_s generally decreases with increasing pl and asymptotically approaches a minimal value for high values of pl. Figure 11 gives two examples for electrode protrusions in SF_6 as broken curves.

Streamer propagation is controlled by a field criterion that requires that the background field in which the streamer propagates exceed a threshold value, which is referred to as the stability or propagation field E_p. It has been shown by numerical simulations that this field also approximately indicates the average field that is established in the streamer channel during propagation (8). E_p is approximately proportional to the critical field E_c, so that the streamer propagation condition can be expressed as

$$E > E_p \approx E_c \gamma(\text{gas, polarity}) \quad (5)$$

with a dimensionless proportionality factor γ that generally depends on the gas and the streamer polarity. Table 1 gives approximately numerical values of γ for SF_6 and air.

The distance L_s to which a streamer propagates is determined by the distribution $E(x)$ of the electric field along the propagation path and is given, according to (9), by the integral relation

$$U = E_p L_s + \int_{L_s}^{D} E(x)\,dx \quad (6)$$

where U is the voltage applied across the gap and D the gap distance. In the limit of small insulation defects of scale 1 embedded in a locally uniform background field E_0 this relation reduces to the approximate expression

$$L_s \approx l(E_0/E_p)/[1-(E_0/E_p)] \quad (7)$$

The propagation length of the streamer L_s is thus approximately proportional to the length scale l of the defect and to the field ratio (E_0/E_p) in the limit $(E_0/E_p) \ll 1$.

Due to the emission of ionizing photons from the streamer tip, streamers have the tendency to initiate parallel streamers from their starting electrode and to branch. For this reason streamers normally do not occur as single events, but form complex patterns, which are called streamer coronae [Fig. 8(d)]. The charge Q_{co} injected into such a streamer corona can be estimated from its length scale L_s by the dimensional relation

$$Q_c \approx g_{co}\varepsilon_0 L_s(l \cdot E_0) \approx [g_{co}\varepsilon_0/E_p](l \cdot E_0)^2/[1-(E_0/E_p)] \quad (8)$$

where g_{co} is a dimensionless geometry factor depending on the geometrical shape of defect and corona, and $\epsilon_0 = 8.85 \times 10^{-12}\ \mathrm{A{\cdot}s{\cdot}V^{-1}{\cdot}m^{-1}}$ is the permittivity of the vacuum. The corona charge Q_c is thus approximately proportional to the square of the product $(E_0 \cdot l)$.

The streamer propagation velocity V_s is determined by the avalanche dynamics at the streamer tip and is typically in the range of several $10^5\ \mathrm{m{\cdot}s^{-1}}$ to $10^6\ \mathrm{m{\cdot}s^{-1}}$ (see vol. 4, p.123).

The significance of streamers for gas insulation is manifold:

- Streamer corona bursts are partial discharges that can be detected by pd measurement devices (see vol. 15, p.648) and therefore can serve as defect indicators in quality control and insulation monitoring.
- Permanent streamer discharge activity may lead to gas decomposition and degradation of insulation surfaces.
- Streamers are necessary pre-stages of more intensive discharge types such as leaders and sparks. The streamer criterion therefore is a necessary but not sufficient criterion for gas insulation breakdown.

Leaders. Leaders develop from a streamer corona by heating one or more of the streamers to a threshold temperature above which an efficient electron production mechanism is activated. A channel with enhanced electronic conductivity is thus formed, which acts like a conducting protrusion and carries the electrode potential into the discharge gap. It thereby enhances the streamer activity at the leader tip. The related corona current is fed into the channel and causes further heating so that the process becomes self-propagating [Fig. 8(e)].

Several streamer-to-leader transition mechanisms have been identified of which the precursor and the stem mechanism [Pr and St in Fig. 8(d)] are the most important ones for gas insulation (9). The precursor mechanism is active in weakly branched (bushlike) coronae and is initiated by a local bipolar ion drift process at the tip of the strongest streamer. This mechanism leads to a stepped leader propagation mode in the form of a sequence of subsequent streamer coronae [St in Fig. 8(e)]. The stem mechanism is active in strongly branched (treelike) coronae and consists in heating a common stem to which the currents from many streamer branches are channeled. This mechanism normally leads to a continuous leader propagation [C in Fig. 8(e)]. For details see vol. 4, p. 132.

The key quantity controlling leader inception is the space charge developed by a streamer. An approximate measure for this charge is the total charge Q_c of the corona, which can be used to formulate an integral leader inception criterion of the form

$$Q_{co} > Q_l(\text{inception mechanism, gas, } p, \text{ polarity, corona and gap geometry}) \quad (9)$$

Here, Q_l is a critical corona charge value that the corona charge Q_{co} has to exceed so that the strongest of the corona streamers is transformed into a leader section. Q_l generally depends on the gas, its pressure p, and the discharge polarity. Moreover, it is affected by the geometry of the disturbance from which the corona has developped and by the particular features of the streamer-to-leader transformation mechanism. Q_l is generally decreases with increasing pressure p and is higher for negative polarity than for positive polarity.

The leader channel is a non-equilibrium plasma, heated to a temperature of a few thousand Kelvin. Due to the overpressure developed by the heating, the leader channel expands radially. Its conductivity is determined by a field-controlled equilibrium between collisional ionization, attachment, and field detachment. The related leader channel field is controlled by the gas density within the heated and expanding channel (9, 10). According to Ref. 11 its av-

erage value E_{lc} scales approximately as

$$E_{lc} \approx c_{lc}(\text{gas, polarity, } p)/t \quad (10)$$

where t is the age of the leader channel. The proportionality factor c_{lc} depends mainly on the gas, the polarity, and the leader propagation speed and only weakly on the gas pressure p.

The leader propagation velocity V_l depends on the gas, increases with gas pressure p and leader tip potential U, and is higher for positive polarity than for negative (9).

$$V_l = V_l(U, \text{ polarity, gas, } p) \quad (11)$$

The main significance of leaders for gas insulation is their role as an intermediate between streamer and breakdown. Whenever the leader–corona system crosses the insulation gap, this unavoidably leads to breakdown, because the leader channel is sufficiently conductive to be rapidly heated to spark temperature.

Breakdown. Both streamers and leaders are pre-ionized channels that, by crossing the insulation gap, establish a conducting path between the electrodes [Fig. 8(f)]. If the field applied to such a channel is sufficient to further enhance the channel conductivity, this will lead to further heating, channel expansion, density reduction, and ionization, so that thermal runaway occurs leading to thermal ionization and formation of a spark plasma with temperatures in the range of 10,000 K to 30,000 K. For engineering purposes the streamer/leader-to-spark transition can be described, to a first approximation, by an average field criterion of the form

$$E_{av} = U/D > E_{ss} \approx E_c f_{ss}(\text{gas}, p, \text{ polarity}, \ldots) \quad (12)$$

where U is the voltage applied over the gap D, so that $E_{av} = U/D$ is the average field applied along the channel and E_{ss} is a critical transition field for spark formation, which can be expressed by a dimensionless factor f_{ss} by referring it to the critical field E_c. A general theory for this transition has not yet been developed. For practical purposes it is sufficient to know, that, for SF_6 insulation, $f_{ss} \ll 1$ for both streamers and leaders. Their gap crossing necessarily triggers breakdown. In outdoor air insulation the same is true for leader crossing, whereas streamer crossing need not always lead to breakdown. In this case the precise value for f_{ss} has to be determined as described in (10, 12) and (13).

Once the spark has been initiated the further decrease of the spark channel resistance R can be approximately quantified by semi-empirical spark laws such as the Toepler spark law (1), which has the form

$$R(t) \approx \frac{k_T D}{\int i\,dt} \quad (13)$$

where k_T is the Toepler constant and $\int i\,dt$ is the charge that has flowed through the channel. Experimentally determined values for k_T are given in Table 1. The time-varying resistance R(t), together with the source impedance of the circuit by which the current is supplied, determines the current surge in the breakdown channel.

Role of Insulator Surfaces. Solid support insulators are necessary components of gas-insulated systems. They experience dielectric stresses inside the solid and may affect gas discharge processes in the vicinity of their surface. Three major surface effects have to be distinguished:

1. Subcritical discharges or partial discharge activity at the electrodes may produce ion flows that land on insulator surfaces so that surface charges are accumulated, which, if large enough, may distort the "as-designed" field in the insulation and thereby cause critical-field enhancements at electrodes leading to breakdown. This effect can be particularly critical in dc insulation systems, but may also occur under ac conditions, because the discharge activity is normally polarity-asymmetric, so that net charges can also accumulate under ac stress. Insulator surface charging is minimized by design measures such as suppressing subcritical discharges by adequate surface finish, by designing the field so that electric field lines do not intercept insulator surfaces, and, in dc systems, by applying weakly conducting coatings on the insulator surface to grade the field distribution ohmically.
2. Gas ionization in the vicinity of an insulator surface may receive contributions from surface processes such as surface ionization and surface attachment, which quantitatively modify the gas discharge characteristics (14, 15).
3. Insulator surfaces may carry conducting contaminants such as weakly conducting surface layers or electrostatically attached particulate contamination. Conducting surface layers may originate from the condensation of conducting liquids such as humidity, from corrosion of the insulator surface, and from the deposition of conducting products, mainly carbon or semiconducting metal compounds. Such conducting surface layers may distort the "as-designed" electrostatic field by ohmic grading and may cause surface leakage currents, which can lead to thermal runaway heating and consequent surface flashover. All these effects are avoided by keeping the humidity sufficiently low, by choosing corrosion-resistant insulator materials, and by avoiding materials and processes that could generate conducting deposits. The cumulation of such measures constitutes an essential part of what is understood by product quality.

Basic Concepts of Gas Insulation Design

The design of gas-insulated systems is an iterative optimization procedure that has to reconcile three major boundary conditions, namely:

1. The desired insulation performance, which is expressed in terms of the test voltages that the system has to support without failure
2. The insulation gas pressure, which is chosen according to required compactness, climatic conditions, and pressurized-enclosure design considerations
3. The technically feasible manufacturing and assembling quality, which is to be expressed in terms of

unavoidable defect scales

The tools available for this optimization process are numerical field calculation methods, and the leading optimization criteria are the defect tolerant design fields for all defect types that may be present in the system and for all voltage stresses to which the equipment will be exposed during testing and operation. Design field relations of the type of Eq. (2) specify the maximally admissible fields in dependence on the gas pressure, the defect type, the defect scales, and the test voltage waveform. They have to be derived from discharge models or experiments. As the full set of design field relations cannot be treated exhaustively here, an example for the derivation of a specific design field relation from a discharge model will be given in the subsection on SF_6 insulation.

SF_6 Insulation

This subsection focuses on three SF_6-specific issues, namely, a discussion of the SF_6-specific discharge processes, an example of the derivation of a defect-tolerant design field relation, and an assessment of the environmental impact of SF_6 power equipment.

SF_6-Specific Gas Discharge Processes. The most important gas discharge processes controlling the performance of SF_6 insulation systems are streamers and leaders. Figure 9 shows photographs of these two discharge types at positive polarity. Figure 9(a) shows a positive streamer corona at the tip of a spherically capped electrode when a voltage below the leader inception level is applied. The streamers approximately follow the electric field lines and form a bush-like pattern that is only weakly branched. The luminous structures at the periphery of the corona are precursors, i.e. pre-stages of leader inception. Figure 9(b) shows a leader discharge in the same gap when a voltage just exceeding the leader inception level is applied. The precursor(s) of the first corona now initiate a leader, which propagates into the gap in the stepped mode as a chain of streamer coronae, each of which emerges from a precursor of the previous corona. At the second step corona, three precursors are seen to form, two of which develop to propagating leaders, so that leader branching occurs. The third one does not make a transition.

The most relevant characteristic of SF_6 streamers is the field in the streamer channel, which is very high and equal to the critical field E_c (see Table 1). The reason for this is the extremely high electron attaching capability of the SF_6 molecule. The high streamer channel field has the important consequence that, according to Eq. (7), the streamer propagation length L_s becomes very low. Streamer coronae in SF_6 therefore are very compact and localized structures, which only extend over a small fraction of the insulation gap. They thus constitute partial discharges, not breakdown. As a consequence, *the partial discharge inception criterion in* SF_6 *is identical with the streamer inception criterion.*

For positive polarity, the most relevant characteristics of positive SF_6 leaders can be summarized by the scaling laws:

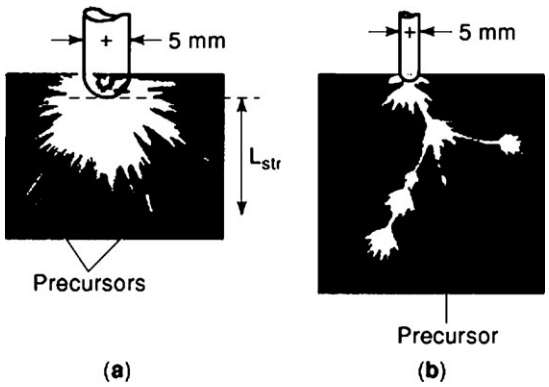

Figure 9. Photographs of a streamer corona and a branched leader in SF_6 with 20% N_2 admixture (to increase luminosity). Point-to-plane gap with hemispherically capped point electrode of 2.5 mm radius. Precursors marked by arrows. (a) Streamer corona below leader inception voltage; (b) branched leader above leader inception voltage.

Average channel field (11):

$$E_{lc} \approx c_{lc}/t \qquad \text{with} \quad c_{lc} \approx 0.2\,\mathrm{V{\cdot}s{\cdot}m^{-1}} \tag{14}$$

Propagation velocity (9):

$$V_l \approx c_{Vl} p\, U^2 \qquad \text{with} \quad c_{Vl} \approx 10^{-11}\,\mathrm{m{\cdot}s^{-1}{\cdot}Pa^{-1}{\cdot}V^{-1}} \tag{15}$$

Under typical conditions in SF_6 insulated systems (namely, pressures of the order of 500 kPa, insulation gaps of the order of 10 cm, and applied voltages of the order of 300 kV) one obtains $V_l \approx 5 \times 10^5\ \mathrm{m{\cdot}s^{-1}} = 50\ \mathrm{cm}/\mu\mathrm{s}$. This corresponds to a gap-crossing time of 200 ns. The average leader field strength after this time is of the order of $E_{lc} \approx 10$ kV/cm, corresponding to a voltage drop of 100 kV across the gap. Thus, a large fraction of the applied voltage U is propagated by the leader into the gap. As a consequence, SF_6 leaders, once initiated, cross the gap in a time much shorter than the duration of most of the voltage transients by which the system may be stressed. SF_6 leaders thus unavoidably lead to breakdown once they have been initiated. Therefore, the general condition for breakdown in compressed SF_6 insulation is the simultaneous fulfillment of both the streamer and leader inception criteria.

Defect-Tolerant Design Fields in SF_6 Insulation. Figure 10 is a repetition of Fig. 3 showing the basic elements of a gas insulation system with some typical defects, which are shown magnified. The surface roughness of the high-voltage electrode can be represented, in a simplified way, as a set of small hemispherically capped protrusions of scale l and tip radius r as indicated in Fig. 10(c). Similarly, a conducting particle that is oriented parallel to the electric field by electrostatic dipole forces and is in contact with the enclosure can be represented as an oblong hemispherically capped protrusion (Fig. 10(a)). A partial delamination of the support insulator from the electrode around which it is moulded can be approximately represented as a gas gap enclosed by a metal and an insulator surface as shown in Fig. 10(b).

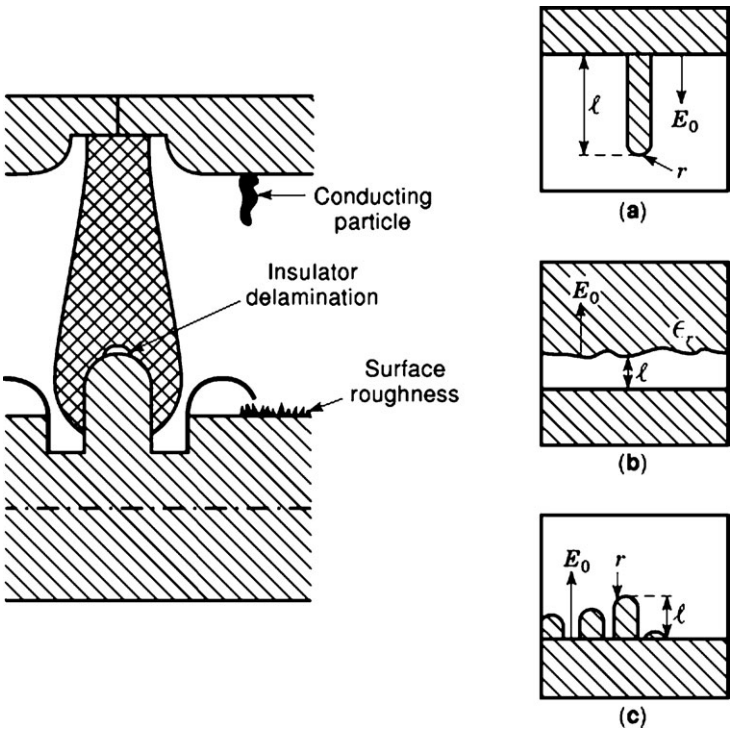

Figure 10. Some typical defects in gas insulated systems and their simplified representation for modeling: (a) conducting particle in contact with an electrode, modeled as electrode protrusion; (b) partial delamination between insulator and electrode, modeled as gas gap between conductor and insulator; (c) surface roughness, modeled as a set of electrode protrusions.

As an example for the derivation of a design field relation we choose the electrode surface roughness and the conducting particle, both of which can be represented as conducting protrusions on an electrode.

We first determine the background field E_{0s} at which streamer inception would take place at the tip of the protrusion. For hemispherically capped protrusions the normalized inception criterion in Eq. (4) takes the specific form

$$E_{0s}/E_c = f_s(pl,\ l/r) \tag{16}$$

where l is the length of the protrusion and r its tip curvature radius. This relation can be determined numerically with the help of the streamer inception criterion Eq. (16) and is plotted in Fig. 11 in the form of broken curves with the aspect ratio l/r as parameter. Surface roughness protrusions have typical aspect ratios $l/r \approx 3$, and particulate contamination typically has $l/r = 30$. The reduced streamer inception field decreases with increasing product pl and increasing aspect ratio l/r.

In order to evaluate the leader inception criterion in Eq. (9), the charge Q_{co} of the corona emerging from a protrusion has to be compared with the leader inception charge Q_l. For positive leaders in SF_6, Q_l obeys the specific scaling law (9)

$$Q_l \approx c_l/p^2 \tag{17}$$

with a proportionality factor c_l of the order of a few 10 A·s·Pa^2. The corona charge Q_{co} has to be determined numerically by a model that represents the shape and extension of the corona for the protrusion geometry (16). This model is limited to oblong protrusions in the range $pl >$ 500 Pa·m. Similarly to streamer inception, the leader inception conditions can also be expressed in the form of a reduced leader inception background field E_{0l}/E_c. The corresponding curves for oblong protrusions with an aspect ratio $l/r = 30$ are represented in Fig. 11 as solid curves for the gas pressures 100 kPa and 500 kPa. In contrast with the streamer inception curves, the leader inception curves do not only depend on the product pl but have an additional, though relatively weak, pressure dependence.

The most important features of the streamer and leader inception curves in Fig. 11 are the following.

For *surface roughness* the aspect ratio l/r of the protrusions is typically around 2–3 and the product pl is the range below 100 Pa·m for typical gas pressures of several hundred kilopascals and roughness scales up to about 100 μm. In this parameter range only the streamer inception fields can be reliably calculated. They are found to lie very close to the experimental breakdown data. Hence, *at rough electrodes in compressed SF_6 insulation, the streamer criterion is a necessary and suficient breakdown criterion.*

For oblong *particles* the aspect ratio l/r is typically 10 to 50. With gas pressures of several hundred kilopascals and particle lengths of several millimeters, the product pl is typically in the range 10^3 Pa·m to 10^4 Pa·m. In this range the streamer inception field is seen to be much lower than the leader inception field. Thus:

In the presence of particulate contamination in compressed SF_6 insulation the breakdown criterion is the leader criterion.

Below the breakdown level, partial discharge activity occurs, the inception of which is controlled by the streamer criterion.

The following general conclusions for SF_6 insulation design can be drawn from the example discussed above:

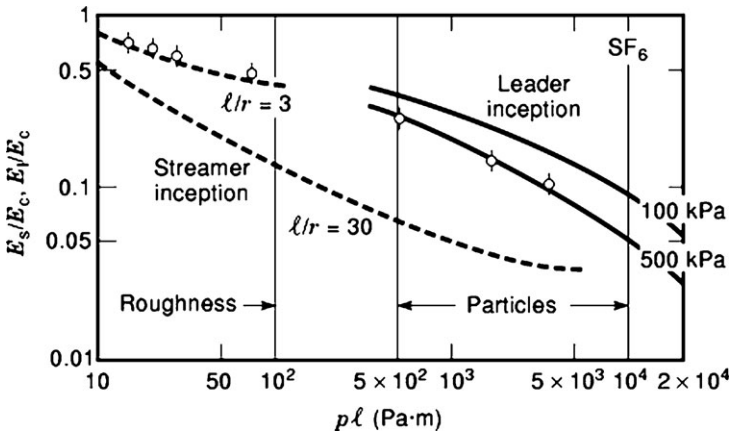

Figure 11. Reduced background fields at which streamer and positive polarity leader inception takes place in SF_6 in dependence on the product pl: E_s/E_c and E_l/E_c are the reduced streamer and leader inception fields (broken and solid curves, respectively); p = gas pressure; l = protrusion length scale; l/r = protrusion aspect ratio. $l/r \approx 3$ corresponds to surface roughness; $l/r \approx 30$ is typical for conducting particles. Leader inception curves have an additional pressure dependence as indicated for 100 kPa and 500 kPa. Points are experimental data.

- The degree to which the theoretical insulation capability of SF_6 (as given by its critical field) can be exploited in practice depends strongly on the size of the defects, i.e., is controlled by the quality of equipment manufacturing, assembling, and by defect control during equipment erection.
- The design field relation for protrusion-type defects such as surface roughness and particulate contamination is given by a combination of the streamer and the leader inception curves.
- Design field relations for other defect types can be derived in a similar way.
- In the presence of particulate contamination the streamer inception level is substantially lower than the leader inception level. This enables a consistent design and quality control philosophy by which defects that exceed a "designed-for" size can be detected by pd measurements, i.e. by nondestructive testing.

Environmental Aspects of SF_6 Insulation. Whereas SF_6, being a chlorine-free molecule, does not deplete stratospheric ozone, it is a very potent greenhouse gas (17). Its environmental impact therefore has to be evaluated carefully and has to be weighed against its undoubted functional advantages as insulation and switching medium.

The relative importance of SF_6 with respect to other greenhouse gases, predominantly CO_2, has to be quantified in the first instance. This has been done in Ref. 17, where it was shown that all the SF_6 hitherto released into the atmosphere contributes less than 0.1% to the total greenhouse effect caused by all man-made gas emissions. In the same reference, also the future SF_6 emissions from electric power equipment due to leakage and handling losses were estimated and found to increase the SF_6 contribution to less than 0.2% till the end of the next century. In spite of its very high nominal greenhouse potential, the SF_6 used in TRD equipment is thus seen to be environmentally irrelevant from a quantitative point of view due to the very small quantity in which it is produced, used and released.

The relative role of SF_6 in the total environmental impact of electric power equipment has to be determined in the frame of an integral environmental impact analysis of a functional unit of T&D equipment. The procedure for such an analysis is described in the international standard ISO 14000 on environmental life cycle analysis (*LCA*), which will be briefly discussed in the technology outlook section. LCA applied to SF_6-insulated power equipment shows that the excellent insulation and switching capability of the gas allows one to render the equipment so compact that the environmental impact of the released SF_6 is overcompensated by the savings of other materials and their environmental impact.

In spite of its environmental insignificance at present, environmentally correct handling and recycling of SF_6 is an important issue under the long-term aspect because the gas has a long atmospheric lifetime of the order of 3000 years. Under this aspect, SF_6 losses to the atmosphere have to be minimized. Losses from electric power equipment occur by leakage during the operating life and by gas handling during manufacturing, commissioning, maintenance, and decommissioning of equipment. With present equipment design the lifetime leakage losses can be kept below 12%. Also, the lifecycle gas handling losses can be limited to less than 2% when the presently available gas handling equipment and practice are systematically applied. Thus, total life cycle losses below 15% can already be achieved today and have potential for further reduction in the future. In order to encourage correct SF_6 handling and recycling in electric power equipment, recent committee publications (18–23) provide guidelines and references.

SF_6 CIRCUIT BREAKERS

Among the various types of gas circuit breakers, the axial flow cooling principle is most frequently applied in SF_6 circuit breakers. The main processes in this type of circuit breaker will therefore be discussed in some more detail. A comprehensive treatment can be found in Refs. 4–6.

Arc Interruption Process

Arc interruption in axial-flow breakers is controlled by a complex interaction of thermal, gas flow, and dielectric processes, which can only be modeled quantitatively by detailed numerical simulation. The discussion presented here will be strongly simplified and will only highlight the major effects and design-relevant parameters. For quantitative details the reader is referred to Ref. 24 and 25.

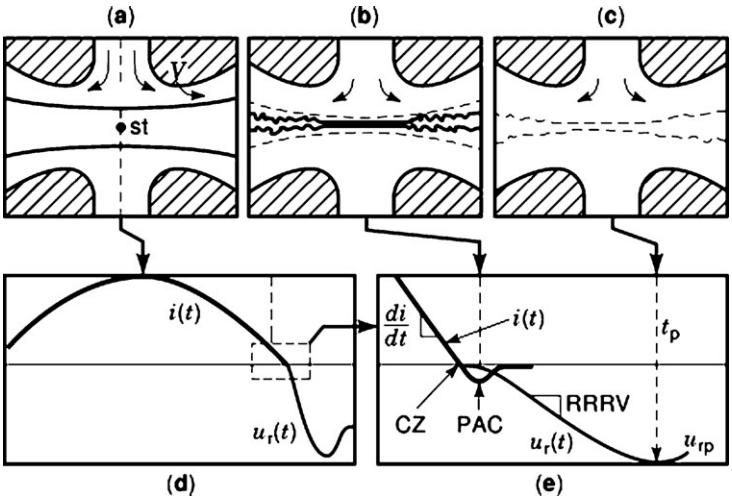

Figure 12. Phases of current interruption in a gas circuit breaker with axial gas flow cooling. Arc-flow configuration (a) during the high-current phase and (b) during the post-arc-current (PAC) phase. (c) Residual hot gas channel configuration during the dielectric recovery phase. (d) Current half wave $i(t)$ prior to arc interruption, and recovery voltage $u_r(t)$ after arc interruption. (e) Expanded representation of current and recovery voltage in the vicinity of current zero (CZ) showing the post-arc current (PAC), the current ramp (di/dt) prior to CZ, and the characteristics of the recovery voltage (RV) after CZ: rate of rise of the recovery voltage (RRRV) and peak value u_{rp} at time t_p.

The phases of the arc interruption process are schematically represented in Fig. 12. The arcing phenomena in the breaker can be broken down into three main phases, which are correlated with the current $i(t)$ flowing through the arc and the recovery voltage $u_r(t)$ appearing across the circuit breaker terminals after the current has been interrupted at a natural current zero (*CZ*) of the ac current [Fig. 12(d) and 12(e)].

High-Current Phase. Figure 12(a) shows the arc during the high-current phase when it is controlled by the imposed axial gas flow as indicated by the arrows. Depending on the magnitude of the current, the flow may be modified by nozzle material that is vaporized from the nozzle surface (arrow V). The arc cross section A_a at the stagnation point st is determined by a convective energy balance in which the ohmic heat dissipated in the arc is carried away by the plasma flow through the nozzles (21). The arc cross section A_a then scales as

$$A_a \approx c_a (L_n/p_0)^{1/2} i \qquad (18)$$

where $c_a \approx 7 \times 10^{-5}$ $m^{3/2}\cdot Pa^{1/2}\cdot A^{-1}$ is a gas-specific constant, L_n the average distance between the stagnation point st of the flow and the nozzle throats, and p_0 the stagnation pressure in the high-pressure reservoir from which the flow is driven. Equation (18) provides a design relation to determine the nozzle throat cross section required to accommodate the arc if the stagnation pressure and the maximal current to be handled by the circuit breaker are prescribed.

Thermal Interruption

Figure 12(b) shows the arc in the vicinity of a CZ. Due to the low current, the arc has a small cross section through which a residual current, the postarc current (*PAC*), is driven by the rising recovery voltage $u_r(t)$. The interruption of the PAC requires that the arc plasma be cooled to below the temperature at which the plasma conductivity ceases, about 5000 K in the case of SF_6. The cooling process is controlled by the thermal energy balance of the arc during the PAC phase, in which the energy losses by flow cooling compete with ohmic reheating of the arc channel by the PAC. In axially cooled SF_6 breakers the PAC has a duration of the order of a microsecond (27, 28). Once interrupted, the arc leaves behind a nonconducting hot gas channel, which is schematically indicated in the figure by a dotted contour and which has an initial temperature of about 4000 K at the end of the PAC phase.

The thermal interruption capability can be quantitatively related to the main design features of the circuit breaker by numerical simulations at various levels of detail (e.g., Refs. 27–29). The simplest approach is an integral energy balance consideration, which leads to a differential equation for the arc conductance G of the form

$$(dG/dt)/G = (1/\tau)[(u_r(t)\cdot i)/P_{cool} - 1] \qquad (19)$$

The parameters τ and P_{cool} characterize the cooling efficiency of the gas flow and are related to the flow-driving stagnation pressure p_0. Solving this equation together with the mesh equations of the electric circuit from which the arc current is fed yields the PAC and the success or failure of the thermal interruption process. For a detailed discussion of this type of model see Ref. 27.

For practical purposes it is convenient to represent the results of thermal arc interruption experiments or model calculations in the form of *thermal interruption limit curves* (e.g. Ref. 24, 27). They give, for a specific breaker design, a relation between the two main interruption stress factors, namely, the steepness di/dt with which the current is ramped down to CZ [Fig. 11(e)] and the initial rate of rise of the recovery voltage, (RRRV) $(du/dt)_0$, after CZ [Fig. 11(e)]. A combination of di/dt and $(du/dt)_0$ can only be interrupted when the corresponding point in the di/dt - $(du/dt)_0$ - plane lies below the limit curve. For the usual sinusoidal ac current, the current ramp is given by $di/dt = \omega I$, where ω is the angular frequency of the ac voltage and I the effective value of the current.

The most important parameters of the thermal limit curve are the kind of gas and the stagnation pressure p_0 driving the gas flow. Figure 13 shows a plot of the thermal interrupting limit curves for SF_6 and air for a stagnation pressure of $p_0 = 1.5$ MPa (19). It is seen that both curves decay with increasing RRRV and that the interruption capability of air is much lower than that of SF_6. The limit curves, including their pressure dependence, can be interpolated by an analytical expression of the form

$$\mathrm{RRRV} \approx c_t p^n \left(\frac{di}{dt}\right)^{-m} \qquad (20)$$

where the exponents m and n and the proportionality constant c_t are determined by fitting to numerical calculations

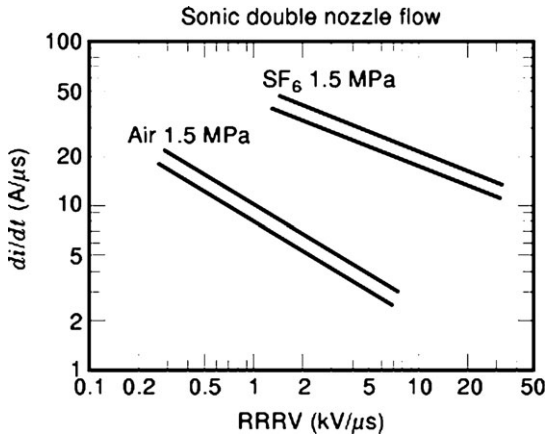

Figure 13. Thermal interruption limit curves for SF_6 and air. Arc with axial gas flow cooling and sonic flow in the nozzle throat. Flow-driving stagnation pressure, 1.5 MPa. Hatched areas indicate scatter of measurements.

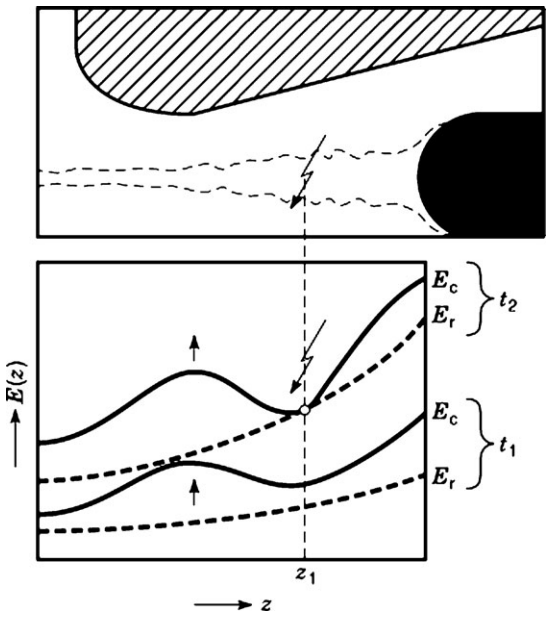

Figure 14. Schematic representation of dielectric recovery process. Axial distributions of the critical field $E_c(z)$ in the hot gas channel and the applied field $E_r(z)$ due to the recovery voltage $u_r(t)$. Both field distributions are schematically represented at two successive times t_1 and t_2. For $t = t_1, E_r < E_c$ all along the channel: no dielectric failure. For $t = t_2, E_r$ reaches E_c at location z_1: dielectric failure initiated at z_1.

or experimental data. As the exponent n is positive, an increase of the flow-driving stagnation pressure p_0 shifts the limit curves to higher values, i.e. increases the thermal interruption capacity.

The thermal interruption performance is critical for circuit conditions at which high currents are followed by steeply rising recovery voltages. The most critical case is normally the so-called short line fault (*SLF*), when a short circuit occurs on a HV transmission line at a distance of the order of 1 km from the substation. Such a fault is characterized by an extremely high RRRV, which is generated by traveling wave phenomena on the line. This switching case usually determines the short-circuit current interruption limit of the circuit breaker. The main design parameter by which this limit can be influenced is the flow-driving stagnation pressure p_0.

Dielectric Recovery

Figure 12(c) shows the phase after successful thermal interruption, which is referred to as the dielectric recovery phase. The pressure distribution $p(z)$ along the hot gas channel is imposed by the stagnation pressure p_0 and the nozzle contour and remains approximately constant in time during the dielectric recovery phase. The hot gas channel left by the arc (dotted contour in the figure) is cooled by the same flow mechanisms as in the thermal recovery phase but without further energy input, as the post-arc current has been interrupted. The flow cooling causes the temperature distribution $T(z, t)$ along the channel to decrease with time.

The quantity which determines the dielectric strength of the hot gas channel, i.e. its critical field E_c, is the molecular particle density n. It varies along the channel according to the gas pressure $p(z)$ and the temperature $T(z, t)$ according to the gas-kinetic relation $p = nkT$. The resulting molecular particle density distribution $n(z, t) = p(z)/[kT(z, t)]$ determines the axial distribution of the critical field E_c, which, according to Eq. (2), is

$$E_c(z,t) = \left(\frac{E}{n}\right)_c n(z,t) = \left(\frac{E}{n}\right)_c \frac{p(z)}{kT(z,t)} \tag{21}$$

$(E/n)_c$ is found to be approximately temperature-independent up to temperatures of about 2000 K (30, 31). The solid curves in Fig. 14 schematically represent $E_c(z, t)$ at two successive times t_1 and t_2 during the dielectric recovery phase.

When the recovery voltage $u_r(t)$ is applied to the channel, it produces an axial field distribution $E_r(z, t)$ that is proportional to $u_r(t)$ and can be expressed as

$$E_r(z,t) = e(z)u_r(t) \tag{22}$$

where $e(z) = E(z)/u_r$ is the voltage-reduced electric field distribution along the contact gap. $E_r(z, t)$ is schematically represented by the broken curves in Fig. 14 for the two successive times t_1 and t_2.

The dielectric recovery of the contact gap is determined by the "race" between the two field distributions $E_c(z, t)$ and $E_r(z, t)$, the first of which increases due to the decrease of the temperature $T(z, t)$ and the second of which increases with the rising recovery voltage $u_r(t)$. As long $E_r(z, t)$ remains below $E_c(z, t)$ all along the channel, the gap withstands dielectrically (time t_1). When $E(z, t)$ reaches $E_c(z, t)$ at some point along the channel, dielectric failure is initiated there (time t_2). It is thus seen that the dielectric recovery of the breaker is controlled by a complex combination of design features, of which the stagnation pressure p_0, the nozzle contour, and the field distribution $e(z)$ in the contact gap are the most important ones. For a quantita-

tive discussion of the dielectric recovery process see Ref. 25.

Dielectric recovery is normally the critical process at the highest short-circuit current which the breaker has to interrupt, i.e. when a short circuit occurs near the power source. This case is referred to as terminal fault (*TF*) and is characterized by a relatively low initial RRRV (so that thermal interruption is not problematic) but a maximal peak recovery voltage u_{rp}. As the latter is directly proportional to the system voltage U_0, the dielectric recovery performance limits the system voltage performance of the circuit breaker.

SF_6 Decomposition by Arcs

SF_6 is one of the few gases that are arcing-stable, that is that, after having been desintegrated to atoms and ions by an arc, they recompose to their original chemical structure after the gas has cooled down to ambient temperature. Pure SF_6 by itself would thus completely recombine. It can only decompose when contaminants are made available that are able to react with thermally dissociated SF_6 fragments. The rate at which SF_6 decomposes in a breaker is therefore not an inherent property of the gas but is determined by the quantity in which reaction partners are made available. In gas insulation compartments the decomposition of SF_6 by partial discharge activity and subsequent reaction with trace contaminants such as humidity is so low that the resulting decomposition products, although toxic, are insignificant as health risks (3). In circuit breakers the decomposition rate is substantially higher, as it is determined by arc-eroded materials, mainly from contacts and nozzles. In this case the SF_6 decomposition rate depends on contact and nozzle design.

SF_6 Decomposition in Normally Operating Circuit Breakers. In normally operating SF_6 circuit breakers the reactive contaminants generated by arc erosion are mainly copper (Cu) and tungsten (W) from the arcing contacts and carbon (C) and fluorine (F) from polytetrafluorethylene (*PTFE*) nozzles, which has the net stochiometric composition CF_2. With the thermally desintegrated SF_6 these erosion products react in the following way.

$$SF_6 + Cu \rightarrow CuF_2\,(solid) + SF_4\,(gas) \tag{23a}$$

$$3SF_6 + W \rightarrow WF_6\,(gas) + 3SF_4\,(gas) \tag{23b}$$

$$SF_6 + CF_2 \rightarrow CF_4\,(gas) + SF_4\,(gas) \tag{23c}$$

The reaction products WF_6 and SF_4 further react with trace humidity:

$$SF_4 + H_2O \rightarrow SOF_2\,(gas) + 2HF\,(gas) \tag{24a}$$

$$WF_6 + H_2O \rightarrow WO_xF_y\,(solid) + zHF\,(gas) \tag{24b}$$

$$SOF_2 + H_2O \rightarrow SO_2 + HF\,(gas) \tag{24c}$$

The resulting solid end products are thus the fluoride CuF_2 and the tungsten oxifluorides WO_xF_y. They are usually referred to as *switching dust* and are nonconducting, so that they do not deteriorate the insulation. The main gaseous end products are CF_4, which is inert like SF_6, and the gases SOF_2, SO_2, and HF, which are toxic and partly corrosive.

The rate at which materials are eroded by the arc can be roughly approximated by an erosion law of the form

$$M_i = \frac{m_i}{\mu_i} = \frac{R_i(I)Q_{arc}}{\mu_i} \tag{25}$$

where M_i and m_i are the produced molar quantity and mass, respectively, of the eroded substance i measured in kilomoles and kilograms, respectively, μ_i its molecular weight, $R_i(I)$ its mass erosion rate measured in $kg{\cdot}A^{-1}{\cdot}s^{-1}$, and Q_{arc} the cumulated arcing-current time integral. The mass erosion rate $R_i(I)$ depends on the design of the breaker and increases with the switching current I.

By combining Eq. (25) with the stochiometry of the reaction Eqs. (23) and (24), the decomposition rate of SF_6 and the corresponding generation rates of decomposition products can be quantified. As an example, the decomposition rate of SF_6 due to the erosion of copper–tungsten arcing contacts with a weight composition of 80% W and 20% Cu is found to be

$$V_{N\,SF_6} \approx -360R_cQ \tag{26}$$

where the decomposed SF_6 quantity has been converted to a gas volume $V_{N\,SF_6}$ measured in liters at *STP* (standard temperature and pressure: 20 °C and 100 kPa). As an example, at typical short-circuit current levels in HV breakers, the contact erosion rates R_c are of order 10^{-6} $kg{\cdot}A^{-1}{\cdot}s^{-1}$. After 10 short-circuit operations at 50 kA with 20 ms arc duration, the cumulated current time integral is, for both contacts, $Q = 2 \times 10{,}000$ as the decomposed SF_6 quantity becomes $V_{N\,SF_6} \approx 7$ liters at STP. This is less than 2% of the total SF_6 content of the breaker, which is typically of the order of 500 liters at STP.

Failure Arcing. Failure arcs occur in the rare event of insulation breakdown or circuit breaker failure and are frequently characterized by high currents and long arcing times. As the arc burns between conductors that are not designed for low arc erosion (aluminium, steel, and copper), the gas decomposition is much higher than in normally operating circuit breakers, and the SF_6 is degraded to such a degree that it has to be changed. The large quantities of solid decomposition products that are generated require special safety precautions for personnel doing the repair work.

Health Risk Mitigation. Health risk analysis and mitigation is an integral part of electrical power equipment design, whatever insulation material is used. As opposed to open equipment, systems contained in grounded enclosures exclude electrocution hazards and strongly reduce exposure of personnel to electromagnetic fields, as the grounded enclosure carries most of the return current and compensates the magnetic field of the HV conductor.

With respect to the SF_6-specific toxic and corrosive decomposition products, the following risk mitigation measures are applied (22, 23):

1. SF_6 decomposition products have characteristic smells (pungent for SO_2, acrid for HF, and rotten-egg

for SOF_2) by which they can be noticed at concentrations far below the health risk level. Smell thus provides an efficient and sensitive warning to personnel.
2. In systems that have not experienced arcing, the concentrations of toxic decomposition products remain so low that they are irrelevant to health, so that specific safety measures are not required. Moreover, the equipment is normally furnished with adsorbers for humidity control, which also adsorb decomposition products in case they should have been created by partial discharges.
3. In circuit breakers the generation of decomposition products is inherently unavoidable because of arc erosion. Toxic health risk due to gaseous decomposition products is mitigated by adsorbers, which are designed to remove all toxic and reactive gases that may be generated during the operational life cycle of the breaker. Solid decomposition products are risk-relevant because they may carry adsorbed corrosive gases. They can only be removed when the equipment is opened. In this case specific safety procedures have to be observed by the service personnel to avoid skin contact and inhalation (gloves, dust filter masks, etc.).
4. In the case of rarely occurring internal arc faults or circuit breaker failures, the quantities of toxic and corrosive products may be high, so that service personnel repairing the equipment need improved protection (overalls, respirators).

TECHNOLOGY OUTLOOK

Present day SF_6-based T&D equipment is a mature technology that has been optimized over more than three decades. In the foreseeable future this technology will remain the main technically and environmentally rational choice for most applications. Only in the long term future may new technologies emerge that modify the pattern of SF_6 applications, particularly with respect to the switching function.

The development of T&D equipment is mainly driven by requirements for

- Improved unit performance
- Better performance-to-cost ratio
- Higher reliability
- Lower life cycle cost (longer lifetime, lower service requirements)
- Reduced size, real estate demand, visual impact
- Reduced environmental impact
- Reduced electromagnetic field exposure of personnel

The means to reach these goals are

- Improved in-service monitoring
- Improved (intelligent) control of the equipment in service
- Further exploitation of the insulation capability of SF_6 through reduced defect scales by improved manufacturing quality control

Although the practical implementation of the above development trends will still require substantial product development work, they are rather straightforward in principle and will therefore not be discussed further. It may be sufficient to state that there still is considerable potential to reduce the quantity of SF_6 required per function, which will result in still more compact equipment, lower manufacturing cost, and, as a consequence, less environmental impact. As the last issue is playing an increasingly important role in the public discussion, its methodological aspects will be briefly discussed below before entering technological issues.

Environmental Impact Assessment

The assessment of a technology is a complex task in which technical, economic, political, and environmental issues are interwoven. Three major value groups can be distinguished, namely,

1. Economic values perceived by the user of the technology such as cost, reliability, and life cycle cost (including installation, maintenance, repair, and decommissioning)
2. Nonmaterial values such as reduced health hazard and visual impact
3. Environmental impact

As values 1 and 2 are determined by usual technical and economic principles, we will only discuss the environmental impact in some more detail. The method with which it can be quantified is documented in the international standard ISO 14000 on environmental LCA (32). The main steps of LCA are presented in Table 2 and consist of 5 procedural steps.

Firstly, the *system limits* of a functional equipment unit have to be identified. For T&D equipment this unit is usually a three-phase switching bay or ring main unit as represented in Fig. 2.

Secondly, the *performance* of this unit has to be specified. For switchgear these are rated current and voltage and short circuit interruption performance.

Thirdly, *inventories* have to be established for the resources used, i.e. the materials required, the energies dissipated, and the emissions caused. These inventories have to be established over the full life cycle of the unit, ("cradle to grave") including the production of the materials that are employed, transportation, manufacturing, commissioning, operating lifetime of the equipment, and decommissioning and scrapping at the end of life of the equipment (including recycling of materials).

In the next step, these data have to be weighted by environmentally relevant indicators which account for resource depletion, energies spent for production and recycling, scarcity of used materials and atmospheric impact of emissions like global warming, stratospheric ozone depletion, acidification and smog generation.

Table 2. Environmental impact assessment of T&D technologies according to ISO Standard 14000 on environmental lifecycle analysis (LCA) (32)

1. Identify system limits	
2. Define system performance	
3. Establish environmentally relevant performance features	– Determine "cradle to grave" inventories of – Resources consumed – Energies dissipated – Emission caused
4. Choose a quantitative system of environmental indicators	
	– Scarcity of materials used – Energy spent in production – GWP (→ global warming potential) – ODP (→ ozone depletion potential) – AP (→ acidification potential ("acid rain")) – POCP (→ smog generation)
5. Derive a quantitative judgement	Weight step 3 data with step 4 indicators to quantify ELU (environmental load units)

Finally an *environmental value system* has to be applied to the weighted inventories to derive a quantitative measure for the environmental impact. In this way, all environmentally relevant aspects of the technology are quantified in a reproducible and verifiable manner and the contributions of the various system components to the total environmental impact can be identified. In particular, LCA allows one to determine the role of insulation materials such as gases in comparison to the other materials that are employed to realize the function of a T&D equipment unit.

Development Trends in Gas Insulation

Apart from the ongoing development of SF_6 insulation technology discussed above, it is necessary to determine if there are environmentally rational alternatives to SF_6. Two major such alternatives have been discussed, namely, SF_6 dilution and a complete replacement of SF_6 by another gas.

SF_6 Dilution. It has been suggested to reduce the SF_6 quantity in large gas-insulated systems for both environmental and economical reasons by exploiting what is termed a synergetic gas mixture (33). Synergetic gas mixtures are characterized by an over-proportional influence of the dielectrically better component on the insulation performance of the mixture. The strongest synergy has hitherto been observed between nitrogen and SF_6. The effect is demonstrated by Fig. 15, which shows the critical field E_c of the mixture normalized to the critical field $E_c(SF_6)$ of pure SF_6 in dependence on the SF_6 content of the mixture. It is seen that dilution of SF_6 down to 10% still retains 65% of the dielectric strength of pure SF_6.

For the understanding of the gas discharge phenomena in diluted SF_6 it is essential to note that down to SF_6 contents of only 2% by volume the mixture still behaves as a strongly electronegative gas (34), so that the discharge mechanisms are similar to those in pure SF_6, apart from the quantitative value of the critical field E_c. The insulation design for SF_6–N_2 mixtures can therefore be handled by the same concepts as for pure SF_6. In particular, the normalized streamer and leader inception curves of the kind shown in Fig. 11 and the related design field concept can be

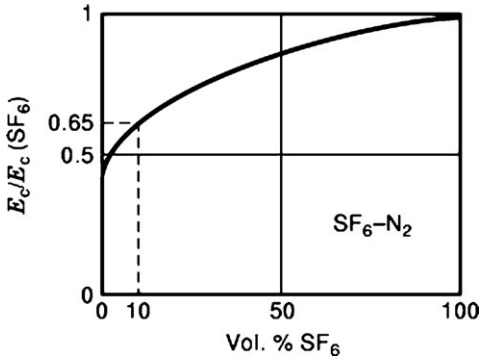

Figure 15. SF_6–N_2 mixture synergy: critical field of SF_6–N_2 mixtures in dependence on the volume content of SF_6.

used in the same way as for SF_6. As an example, the curves in Fig. 16 show the predicted particle-tolerant design field for *LI* (lightning impulse) stress for a 10% SF_6–90% N_2 mixture in the presence of 3 mm long particles at the anode in dependence on the gas pressure p. The corresponding curve for pure SF_6 has been added for reference. To determine the theoretical curve for the diluted SF_6 it has been assumed that the normalized leader inception curve is the same as for pure SF_6 (see Fig. 11). The curves show that for both the pure and the diluted SF_6 the design fields tend to saturate at pressures in the typical gas insulation range around 500 kPa. The points are measurements obtained in a uniform field gap with a 3 mm long protrusion at the anode and are in agreement with the calculated curves.

In the meantime a few prototype gas insulated HV lines with SF_6–N_2 mixtures have demonstrated technical feasibility but have not yet led to a wide-spread application.

SF_6 Replacement by Other Gases. In order to comprehensively explore the possibility of replacing SF_6 by environmentally more favorable insulation gases, a systematic search for such gases is required. In contrast with previous such searches, which were essentially directed towards finding *better* insulation performance than SF_6 (35), the search now also has to include environmental criteria such as low global warming potential (GWP) and ozone depletion potential (ODP), health risk aspects such as nontoxicity and biological inertness, and other LCA-relevant char-

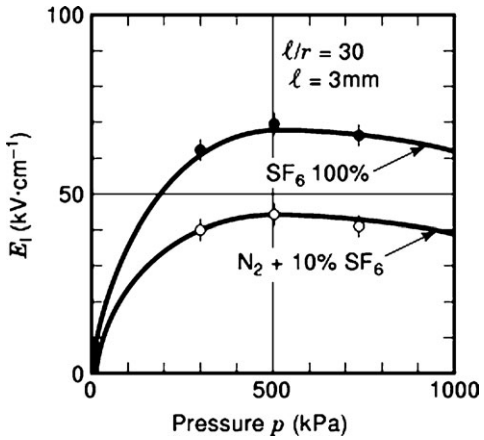

Figure 16. Breakdown field in the presence of an anodic electrode protrusion ($l = 3$ mm, $l/r = 30$) in dependence on the gas pressure p for pure SF_6 and for a mixture of 10% SF_6 and 90% N_2. Solid curves: calculation based on the leader inception curves in Fig. 11. Points: measurements with a 100 ns risetime step voltage pulse applied to a uniform field gap with protrusion.

acteristics. It was shown in Ref. 36 that a combination of chemical systematics and molecular combinatorics allows one to explore the chemically possible gaseous compounds comprehensively. A selection of candidate gases thus identified is represented in Table 3 to illustrate some of the main correlations and trends. The data in the table show that, generally:

- Fluorination is an indispensable (yet not sufficient) condition for high insulation performance. Nonfluorinated gases do not significantly exceed the performance of air.
- High insulation performance is strongly correlated with high molecular complexity, which, however, also tends to entail high GWP, as complex molecular structure is associated with strong infrared absorption.
- Another limit to molecular complexity is defined by the nonliquefaction condition: The more complex a molecule is, the higher its boiling point and the more easily it liquefies.
- The requirements of biological inertness, nontoxicity, and thermochemical stability tend to imply long atmospheric lifetimes, which positively correlate with a high GWP.

In particular, Table 3 shows that

- The perfluorinated gases (group 2) are no alternatives to SF_6, because they, too, have high GWP and tend to decompose or even carbonize or under discharge activity. Only SF_6 and CF_3SF_5 do not carbonize, because they bind discharge-generated carbon in the form of CF_4.
- None of the nonfluorinated gases (group 4) comes close to the performance of SF_6.
- The noble gases (group 3) have to be excluded because their dielectric strength is substantially lower than that of air.
- Among the nonfluorinated gases (group 4), only N_2O has a somewhat better dielectric performance than air. This gas has to be excluded, however, because it is an exothermal compound and has the tendency to decompose explosively.
- The only remaining choices are air and nitrogen, which, however, have an insulation performance only about one-third that of SF_6. Nevertheless, their insulation characteristics will be briefly reviewed below.

Compressed-Air–Nitrogen Insulation. The development of compressed air-insulated switchgear (*GIS*), which had been started in the early sixties, was abandoned in favor of SF_6 insulation, mainly because of the high pressures that were required to compensate for the low specific insulation performance of air: More than 1 MPa had to be used for insulation, and up to 3 MPa for switchgear. A reassessment of this technology requires both an improved understanding of the breakdown processes in compressed air and nitrogen and an environmental lifecycle analysis of the design features associated with the high pressure technology.

As breakdown in atmospheric air is quite well understood (see vol. 4, p.123), the extrapolation of this knowledge to higher pressures allows to derive some basic features of compressed air insulation. Most of the discharge mechanisms are qualitatively similar to those in SF_6 with, however, substantial quantitative differences in the gas characteristics as shown in Table 1. A noteworthy qualitative difference from SF_6 exists with respect to streamer propagation. As the streamer propagation field E_{pr} in air is much lower than the critical field E_c, the streamer corona in air is spatially much more extended than in SF_6. Whereas SF_6 streamers are very localized phenomena, air streamers may extend over a large portion of the insulation gap. In the weakly non-uniform field gaps prevailing in compressed gas insulation, this feature gives rise to a further breakdown mechanism: Streamers may cross the gap and initiate breakdown by direct streamer-to-spark transition without the intermediary of a leader.

The conditions under which direct streamer-to-spark transition or leader breakdown control the insulation performance are not yet well understood. At rough electrodes, the available data seem to indicate that, like in SF_6, the streamer inception criterion is also the breakdown criterion (38). In the presence of particulate contamination with length scales of a few millimeters and at pressures between 300 kPa and 900 kPa, preliminary experimental data indicate that breakdown is approximately controlled by an average field criterion, which would suggest that streamer-to-spark transition might be the controlling process (38). Under these conditions the LI design field condition in the presence of a particle at the anode can be roughly expressed by the average-field criterion eq. (12) above with a spark formation field E_{ss} scaling as

$$E_{ss} \approx (E/p)_{ss} \approx 8 \times 10^5\,\mathrm{V \cdot m^{-1} \cdot Pa^{-1}} \qquad (27)$$

With this criterion the performance of compressed air insulation can be compared with that of SF_6 insulation: For a uniform field gap of $D = 10$ cm, a gas pressure of 500 kPa,

Table 3. Candidate Gases for Insulation with SF_6 as Reference Gas

		Environmental		Physicochemical			Insulation and switching			
No.	Gas	GWP (Ref. CO_2)	Toxicity	B.p. at 10^5 Pa (°C)	Sound velocity at 20 °C (m/s)	Decompos. temperature (°C)	Critical field (ref. SF_6)	Conducting solid decompos. products	Arcing stability	Thermal interruption performance[a] (ref. SF_6)
1	SF_6	25,000	No		140	~1200	1.00	None	Yes	1
2	CF_4	6,300	No	128	168	~3000	0.41	C[b]	Yes	1
	C_2F_6	12,500	No	78	156	~2000	0.8	C[b]	No	0.5
	CF_3SF_5		No	24.5	115	420	1.3	None	No	
3	He		No	269	980	–	0.02	Me[b]	Yes	0.05
	Ar		No	186	308	–	0.07	Me[b]		0.01
4	H_2	–	No	253	1300	~2000	0.18	Me[b]	Yes	~100
	N_2	–	No	196	336	~3000	0.30	C, Me[b]	Yes	~0.1
	O_2	–	No	183	313	~2500	0.33	MeO[b]	Yes	
	Air	–	No		330	~2500	0.3	MeO[b]	Yes	~0.15
	CO_2	1	No	78	254	~400	0.3	MeO[b]	Yes	~0.4
	CH_4	24.5	No	164	418	~200	0.43	C, MeO[b]	Yes	~50
	N_2O	320	Narcotic	88	198	~600[c]	0.47	C, MeO[b]	No	

[a] In terms of limit RRRV when current is ramped to zero with 14 A/μs corresponding to an ac current of 26 kA rms at 60 Hz.
[b] Reaction products with arc-eroded materials such as metals (Me) producing metal oxides (MeO) and polymers producing carbon (C).
[c] Explosive decomposition in N_2 and O_2 at ambient temperature possible because compound is exothermic.

and a 3 mm particle on the anode, the positive LI breakdown voltage would be 700 kV for SF_6 (see Fig. 16) and 400 kV for compressed air. In order to attain the same breakdown voltage as with SF_6 at 500 kPa, the air pressure would have to be increased to 900 kPa.

The relevant discharge processes in compressed nitrogen insulation are still less well understood than in air. The few available experimental data indicate that for a given insulation gap and defect scale the insulation performance of nitrogen is about 10% to 20% lower than for air (36). One reason for this is that the nitrogen molecules are not electronegative whereas air contains the electron-attaching oxygen. Another disadvantage of pure nitrogen is its inability to suppress discharge-induced carbonization, which, in air, is taken care of by the oxygen which oxidizes carbon to the gas CO_2.

It thus has to be concluded that air and nitrogen in compressed gas insulation have a functional performance substantially inferior to SF_6, which would have to be compensated by higher containment pressure. The latter requires more material which will have a negative impact in environmental lifecycle analysis. This may explain that, till now, no compressed air or N_2 insulation system has been put in operation.

Development Trends in Switchgear

The historical oil and compressed air switchgear technologies were phased out of production during the last three decades, mainly for reasons of functionality, reliability, life cycle cost, and safety. Present day switchgear technology in HV transmission is mainly based on SF_6. In MV distribution, vacuum circuit breakers (*VCB*) and SF_6 circuit breakers are about equally used. A summary of the development trends in these two technologies is given in reference (44). For the next decade, revolutionary new concepts for switchgear in T&D are not visible. Only at the long-term horizon may new solid-state technologies emerge that might eventually come into use in T&D switching, such as high-temperature superconductors and silicon carbide (SiC) semiconductors.

SF_6 Switchgear. The development of SF_6 switchgear over the last decade has brought a strong increase of unit performance and reliability. The per-break performance of SF_6 HV circuit breakers has improved from an initial 170 kV at 31.5 kA to 275 kV at 50 kA. SF_6 generator circuit breakers (12 kV to 24 kV) have long exceeded their initial 50 kA short-circuit interruption performance, reached 160 kA, and are now heading towards 200 kA. Compact SF_6 distribution switchgear is available up to 24 kV at 31.5 kA interruption performance and has an uprating potential towards 36 kV at 50 kA. The quantity of SF_6 required for a given interruption performance has gone down by typically 20% to 50% over the last two decades. This trend will continue, although at a slower rate.

A major development step in SF_6 switchgear can be expected when intelligent switchgear control will find acceptance. It uses information from the circuit to control the switching process such as to minimize the stresses on the switchgear structure. Application of such control technology could dramatically simplify the design of the arc interruption zone and further reduce the quantity of SF_6 required per function.

Other Switching Gases. Various unsuccessful attempts were made in the past to find switching gases that perform better than SF_6 (39, 40). The main reasons for the difficulty have been understood. Switching gases have to fulfill more stringent conditions than insulation gases: In addition to good insulation performance, they also need to be arcing-stable, to have good thermal interruption performance, and to have a low velocity of sound to allow efficient gas flow generation by piston compression. The data in Table 3 show that a favorable combination of all these requirements is not encountered among the gases listed. Gases such as hydrogen (H_2) and methane (CH_4), although having excellent thermal interruption capability, are characterized by low insulation performance and high velocities of sound. They also do not suppress the formation of conducting arc decomposition products. It thus turns out that the combination of physicochemical properties of SF_6 is not equaled by any other gas. If a non-SF_6 choice had to be made it would be air. Air was, in fact, the only switching gas that was in use before the advent of SF_6. It was abandoned in the seven-

ties because of environmental and reliability problems and because it was no more competitive with SF_6 switchgear.

Vacuum Circuit Breakers. Vacuum circuit breakers (*VCB*) have been developed, over the last three decades, towards 36 kV and 50 kA unit performance. Prototypes for much higher current and voltage performance have been shown to be technically feasible, such as 100 kA at 13.5 kV and 40 kA at 145 kV (45). HV performance of VCB is inherently difficult to achieve due to the nature of the breakdown process between arced vacuum contacts, which is mainly controlled by the absolute voltage and can therefore not reach the per-break voltage performance of SF_6 breakers at competitive cost.

Semiconductors. For application in present ac-based T&D systems, semiconductors have four major inherent handicaps:

1. High forward conduction losses make them unsuited to carry the usual rate currents (typically up to 2000 A in distribution equipment, 4000 A in transmission equipment, and 12,000 A in generator breakers).
2. The low holdoff voltage per element (typically < 10 kV) would require series connection of many elements for system voltages ranging up to 800 kV.
3. Reverse blocking currents are so high that they do not provide a sufficient degree of circuit disconnection and would require an additional mechanical series disconnector.
4. The high cost per unit makes semiconductors economically noncompetitive with the relatively simple electromechanical technology of present gas switchgear.

The above handicaps will not allow semiconductors to play a major role for switching in the present ac-based T&D system apart from some niche applications at low voltages, low rated currents, and high operation cycle requirements.

The only innovation that might eventually play a role in T&D is a change from ac to dc transmission and distribution based on (presently still hypothetical) SiC power transistors of the hetero-bipolar type. They would be able to substantially outperform the presently used silicon-based power semiconductors due to a combination of higher voltage performance per unit, lower forward losses, and substantially lower switching losses (41). However, their realization poses still unsolved technology problems.

High-Temperature Superconductors. High temperature superconductors can be used to limit short-circuit currents by driving the superconductor from the superconducting to the resistive state, e.g. by using the magnetic field of the current to be limited (42) (see ***Superconducting fault current limiters*** As the current-limiting action of a superconductor occurs almost instantaneously, the current can be limited to a low fraction of the inherent short-circuit current that the network would be able to supply. The concept has demonstrated to be practically feasible at the distribution level (43) but encounters severe cost problems.

Superconductors are capable of providing the novel feature of *short-circuit current-free* system operation. They would make short-circuit interruption capability of switchgear obsolete and would reduce the task of the circuit breakers to that of much simpler load break switches. For SF_6 switchgear, this would result in a further substantial reduction of the quantity of SF_6 required per function. The future role of superconductors in T&D systems will essentially depend on the progress in materials technology and on their cost in comparison with the total cost of the T&D system.

BIBLIOGRAPHY

1. J. M. Meek, J. D. Craggs, *Electrical Breakdown of Gases*, New York: Wiley, 1978.
2. E. Kuffel, W. Zaengl, *High Voltage Engineering*, New York: Pergamon, 1984.
3. M. Khalifa, *High Voltage Engineering*, New York: Marcel Dekker, 1990.
4. C. H. Flursheim, *Power Circuit Breaker Theory and Design*, London: Peter Peregrinus, 1975.
5. R. D. Garzon, *High Voltage Circuit Breakers*, New York: Marcel Dekker, 1996.
6. H. M. Ryan, G. R. Jones, *SF_6 Switchgear*, London: Peter Peregrinus, 1989.
7. L. Niemeyer, A generalized approach to partial discharge modeling, *IEEE Trans. Dielectr. Electr. Insul.*, **2**: 510–528, 1995.
8. I. Gallimberti, Breakdown mechanisms in electronegative gases, in *Proc. 5th Int. Symp. Gaseous Dielectrics*, Pergamon, Knoxville: 1987, pp. 61–80.
9. L. Niemeyer, L. Ullrich, N. Wiegart, The mechanism of leader breakdown in electronegative gases, *IEEE Trans. Electr. Insul.*, **24**: 309–324, 1989.
10. I. Gallimberti, The mechanism of the long spark formation, *J. Physique*, **C7** (40): 193–250, 1979.
11. L. Niemeyer, F. Pinnekamp, Leader Discharges in SF_6, *J. Phys. D: Appl. Phys.*, **16**: 1031–1045, 1983.
12. E. Marode, F. Bastien, M. Bakker, A model of the streamer-induced spark formation based on neutral dynamics, *J. Appl. Phys.*, **50** (1): 140–146, 1979.
13. S. Achat, Y. Teisseyre, E. Marode, The scaling of the streamer-to-arc transition in a positive point-to-plane gap with pressure, *J. Phys. D: Appl. Phys.*, **25**: 661–668, 1992.
14. H. F. A. Verhaart, A. J. L. Verhage, Insulator flash-over in SF_6 gas, *Kema Sci. Tech. Rep.*, **6** (9): 179–228, 1988.
15. I. Gallimberti, G. Marchesi, L. Niemeyer, Streamer corona at an insulator surface. In *Proc. 7th Int. Symp. High Voltage Engineering*, Dresden, 1991, Dresden University of Technology, paper 41.10.
16. N. Wiegart, A semi-empirical leader inception model for SF_6. In *Proc. 8th Int. Conf. Gas Discharges and Their Applications*, Oxford: Pergamon, 1985, pp. 227–230.
17. Anonymous, CIGRE WG 23-10, SF_6 and the global atmosphere, *ELECTRA*, **164**: 121–131, 1996.
18. Anonymous, CIGRE WG 23-10, SF_6 recycling guide, *ELECTRA*, **173**: 43–69, 1997.
19. CIGRE brochure # 234 - SF_6 Recycling Guide
20. CIGRE brochure # 276 - Guide for the preparation of customised practical SF_6 handling Instructions

21. IEC Standard 60376 - Specification of technical grade sulfur hexafluoride (SF_6) for use in electrical equipment
22. IEC Standard 60480 - Guidelines for the checking and treatment of sulfur hexafluoride (SF_6) taken from electrical equipment and specifications for its reuse
23. Committee Draft of the IEC Technical Report 62271- High-voltage switchgear and controlgear - Part 303: Use and handling of sulfur hexafluoride (SF_6) in high-voltage switchgear and controlgear
24. W. Hermann *et al.*, Investigation on the physical phenomena around current zero in HV gas blast breakers, *IEEE Trans. Power Appar. Syst.*, **PAS-95**: 1165–1176, 1976.
25. E. Schade *et al.*, Dielectric recovery of an axially blown SF_6 arc after current zero, parts I to III, *IEEE Trans. Plasma Sci.*, **PS-10**: 141–172, 1982.
26. D. T. Tuma, J. J. Lowke, Prediction of properties of arcs stabilized by forced convection, *J. Appl. Phys.*, **46** (8): 3361–3367, 1975.
27. W. Herrmann, K. Ragaller, Theoretical description of the current interruption in HV gas blast breakers, *IEEE Trans. Power Appar. Syst.*, **PAS-96**: 1546–1555, 1977.
28. M. T. C. Fang, Q. Zhuang, X. J. Guo, Current zero behaviour of an SF_6 gas blast arc. Part II: Turbulent flow, *J. Phys. D: Appl. Phys.*, **27**: 74–83, 1994.
29. Anonymous, CIGRE WG13.01, Applications of black box modelling to circuit breakers, *ELECTRA*, **149**: 41–71, 1993.
30. L. Rothard, J. Mastovsky, J. Blaha, Dielectric strength of SF_6 at elevated temperatures, *J. Phys. D: Appl. Phys.*, **14**: 215–216, 1981.
31. L. Rothard *et al.*, Breakdown experiments in air and nitrogen above 1500 K, *J. Phys. D: Appl. Phys.*, **14**: 715–721, 1981.
32. Anonymous, ISO/TC 207/SC 5, Life cycle assessment, synthetised revised draft 14 040, 1995.
33. L. G. Christophorou, R. J. Van Brunt, SF_6/N_2 mixtures, *IEEE Trans. Dielect. Electr. Insul.*, **2**: 952–1003, 1995.
34. I. Gallimberti, G. Marchesi, R. Turri, Corona formation and propagation in weakly and strongly attaching gases. *In 8th Int. Conf. Gas Discharges*, Oxford: Pergamon, 1985, pp. 587–594.
35. L. G. Christophorou *et al.*, Recent advances in gaseous dielectrics at Oak Ridge National Laboratory, *IEEE Trans. Electr. Insul.*, **19**: 550–566, 1984.
36. L. Niemeyer, A systematic search for insulation gases and their environmental evaluation, *Proc. 8th Int. Symp. Gaseous Dielectrics*, Pergamon, Virginia Beach: 1998.
37. S. Berger, Onset of breakdown voltage reduction by electrode surface roughness in air and SF_6, *IEEE Trans. Power Appar. Syst.*, **PAS-95**: 1073–1079, 1976.
38. M. Piemontesi *et al.*, Some aspects of compressed air and nitrogen insulation, *Proc. 8th Int. Symp. Gaseous Dielectrics*, Pergamon, Virginia Beach: 1998.
39. H. O. Noeske, Arc thermal recovery speed in different gases and gas mixtures, *IEEE Trans. Power Appar. Syst.*, **PAS-100**: 4612–4620, 1981.
40. G. Frind *et al.*,Report EPRI EL-284, January 1977.
41. J. W. Palmour *et al.*, Silicon carbide for power devices. *In 1997 IEEE Int. Symp. Power Semiconductor Devices and ICs*, Weimar, 1997, pp. 25–32.
42. U. Balacandrian, Superpower: Superconductivity in electric power, *IEEE Spectrum*, **34** (7): 26–30, 1997.
43. W. Paul *et al.*, Test of 1.2 MVA high-T_c superconducting fault current limiter, *European Conference on Applied Superconductivity (EUCAS)*, Veldhoven, 1997.
44. S. Yanabu, E. Zaima *et al.*, Historical review of high Voltage Switchgear Developments in the 20th Century for Power Transmission and Distribution System in Japan, *IEEE Trans. Power Deliv.*, Vol. **21**, No. 2, April 2006, pp. 659–664.
45. M. Homma, M. Sakaki *et al.*, History of Vacuum Circuit Brakers and Recent Developments in Japan, *IEEE Trans. Diel. And Insul.*, Vol. **13**, No. 1; February 2006, pp. 85–92

LUTZ NIEMEYER
ABB Research Center, Baden, Switzerland